ANALYSIS OF REGENERATIVE BRAKING IN ELECTRIC MACHINES

A Thesis
Presented to
The Academic Faculty

by

Aravind Samba Murthy

In Partial Fulfillment
of the Requirements for the Degree
Master of Science in the
School of Electrical and Computer Engineering

Georgia Institute of Technology
May 2013

ANALYSIS OF REGENERATIVE BRAKING IN ELECTRIC MACHINES

Approved by:

Professor David G Taylor, Advisor
School of Electrical and Computer Engineering
Georgia Institute of Technology

Professor Thomas G Habetler
School of Electrical and Computer Engineering
Georgia Institute of Technology

Professor Yorai Wardi
School of Electrical and Computer Engineering
Georgia Institute of Technology

Date Approved: 3 April 2013

To my mother and grandmother

ACKNOWLEDGEMENTS

This dissertation would not have been possible without the guidance and the help of several individuals who in one way or another contributed and extended their valuable assistance in the preparation and completion of this study.

First and foremost, my utmost gratitude to my advisor, Dr. David G Taylor, whose continuous guidance and support has been invaluable to me. His patience, motivation, enthusiasm, and immense knowledge has helped me during the research and writing of this thesis. I could not have imagined having a better advisor and mentor and it was certainly a pleasure working with him. I have been greatly influenced by his discipline and dedication to his work and look up to him as a role model.

I would like to thank Dr. Thomas G Habetler and Dr. Yorai Wardi, for taking valuable time out of their busy schedules to serve on my thesis reading committee and provide their invaluable suggestions. I would like to acknowledge support from the Department of Energy under Award Number DE-EE0002627. I would also like to thank Dr. Michael J Leamy from the Woodruff School of Mechanical Engineering who is an integral part of the project which funded this research.

Last but not the least, I would like to thank the ones closest to my heart, my family and my fiancée. I thank my mother who has single-handedly supported me since my father's passing away nine years ago, I owe her my everything. I would like to thank my grandmother and sister who have been tremendous emotional supports throughout my life. I would also like to thank my aunts for always being there for my family. I would like to thank my fiancée, Rajatha Bhat, for always being there to cheer me up whenever I was dejected due to the hurdles I faced during the course of my research.

TABLE OF CONTENTS

LIST OF TABLES

LIST OF FIGURES

SUMMARY

All electric machines have two mechanical operations, motoring and braking. The nature of braking can be regenerative, where the kinetic energy of the rotor is converted into electricity and sent back to the power source or non-regenerative, where the source supplies electric power to provide braking. This thesis investigates several critical issues related to regenerative braking in both DC and AC electric machines, including the determination of boundaries in the torque-speed plane defining the regenerative braking capability region and the evaluation of operating points within that capability region that result in maximum regenerative braking recharge current.

Electric machines are used in the powertrains of electric and hybrid-electric vehicles to provide motoring or braking torque in response to the driver's request and power management logic. Since such vehicles carry a limited amount of electrical energy on-board their energy storage systems (such as a battery pack), it is important to conserve as much electrical energy as possible in order to increase the range of travel. Therefore, the concept of regenerative braking is of importance for such vehicles since operating in this mode during a braking event sends power back to the energy storage system thereby replenishing its energy level. Since the electric machine assists the mechanical friction braking system of the vehicle, it results in reduced wear on components within the mechanical friction brake system. As both mechanical friction braking and electric machine braking are used to provide the requested vehicle braking torque, braking strategies which relate to splitting of the braking command between the two braking mechanisms are discussed. The reduction in energy consumption of a test vehicle along different driving schedules while using different braking strategies is also studied.

CHAPTER I

INTRODUCTION

Every electric machine has two mechanical operations, motoring and braking. As shown in Figure 1, quadrants I and III of the torque-speed plane represent the forward and reverse motoring regions of operation, and quadrants IV and II represent the forward and reverse braking regions of operation respectively. Braking is exhibited in three forms: regenerative braking, reverse-voltage braking or plugging, and rheostatic braking (uses an external resistor bank) [4]. In regenerative braking, the kinetic energy of the rotor is converted to electricity and fed back to the power source. The power source can either be a DC power supply (for DC machines) or an AC power supply (for AC machines) or a DC source connected to an appropriate controllable power converter (DC-DC or DC-AC). The method of plugging or reverse voltage braking involves reversal of the voltage applied across the electric machine to assist the back electro-motive force (EMF) in forcing machine currents to flow in the opposite direction to produce braking torque. This implies that energy from the power source is used to provide braking torque. In rheostatic braking, a resistor bank is connected across the electric machine and kinetic energy of the rotor is dissipated as heat in the resistor bank. Therefore, it can be seen that of the three types of electric braking, regenerative braking is the only braking type that sends electricity back to the power source. In the absence of a resistor bank, an electric machine can either exhibit regenerative braking or non-regenerative braking in the form of plugging. Therefore, it is important to identify the feasibility boundaries of regenerative braking within the braking quadrants of an electric machine. The purpose of this thesis is to provide a clear first-principles analysis of regenerative braking capability in converter-controlled

electric machines powered by a DC source.

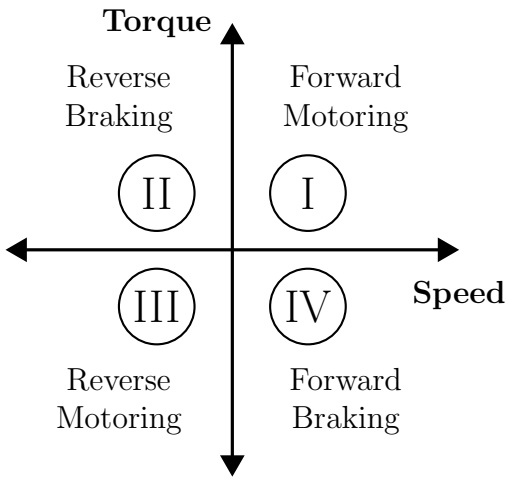

Figure 1: 4-quadrant motoring and braking operations in the torque-speed plane.

The concept of motoring and braking torque-speed capability curves for electric machines has been well established, however the concept of regenerative braking feasibility boundaries remains undocumented in the existing literature. Concepts such as regenerative braking with operating modes that maximize feedback battery power or efficiency, or that maintain constant braking torque, are considered in [6,9], but both papers are based on formulas that apply only to brush-commutated DC machines. In [1, 7], regenerative braking control of permanent magnet synchronous machines controlled by three-phase power converters is studied, but both papers restrict themselves to special operating modes of the power converter and do not fully exploit the capabilities of the system.

Electric machines are commonly used in electric and hybrid-electric vehicle powertrains to provide motoring or braking torque based on the driver's request and power management logic. This makes the concept of regenerative braking all the more important in such vehicles due to the fact that they carry limited electric energy on-board their energy storage systems. Regenerative braking provides a means to generate electric power during a braking event, for immediate use or for storage.

This would reduce the overall energy consumption of the vehicle thereby extending the range of travel of the vehicle for a given energy capacity of an energy storage system. As the electric machine braking assists the mechanical friction brakes attached to the wheels of the vehicle, it results in reduced wear of the components of the mechanical braking system. The effect of this combination of the two braking mechanisms on vehicle stability has been studied in [2] but the limitations imposed by the electric machine system physics has not been considered. A method of using maximum regenerative braking torque for some time during the braking event and smoothly blending out the braking torque to zero at low machine speeds is given in [3, 12], but no physical basis for adopting this method is provided.

Since a combination of electric machine braking and mechanical friction braking is used to provide the required vehicle braking torque, algorithms are devised which relate to the splitting of the braking command between the two braking mechanisms. These algorithms, referred to as braking strategies from now on, are devised to reduce the overall energy consumption of the vehicle by utilizing the knowledge of the regenerative braking capability boundaries. This thesis also analyzes the impact of different braking strategies on the overall energy consumption of a test electric vehicle over different driving schedules.

CHAPTER II

REGENERATIVE BRAKING IN DC MACHINES

2.1 Modeling

The steady-state equivalent circuit diagram of a DC machine with a separately excited field is shown in Figure 2, where v_m is the machine input voltage, i_a is the current through the armature, R_a is the armature resistance, R_c is the core-loss resistance, i_m and i_c represent the magnetizing and core-loss components of the armature current, K_b is the speed constant of the DC machine, i_f is the field current and ω is the angular velocity of the machine. The field circuit is not shown in the above representation. The schematic diagram of the DC machine described above connected to a DC source such as a battery, through a full-bridge DC-DC converter, is shown in Figure 3. The full-bridge DC-DC converter is an actuator used to apply an averaged desired voltage across the terminals of the DC machine. This controllable power converter consists of two legs or half bridges, each consisting of two transistor switches and two diodes as shown in Figure 3. In this circuit diagram, the third terminal of each transistor switch, the control terminal, is not shown. Power is supplied by a DC source, such as an electrochemical battery pack whose steady-state equivalent circuit diagram is shown in Figure 4.

The DC machine is connected across the midpoints of the two converter legs, leg A which is on the left and leg B which is on the right. The output node of leg A has voltage v_A measured with respect to negative supply terminal N and current i_A flows from this leg to the positive motor terminal. The output node of leg B has voltage v_B measured with respect to negative supply terminal N and current i_B flows from this leg to the negative motor terminal. Applying Kirchhoff's voltage law (KVL) and

Kirchhoff's current law (KCL), we obtain the machine voltage and current as

$$v_m = v_A - v_B$$

$$i_a = i_A = -i_B$$

In order to control the instantaneous current in the electric machine, the average voltage applied to the DC machine has to be controlled. The converter achieves this desired function of establishing a desired average machine voltage using pulse-width modulation (PWM), with the switches operating in switched-mode operation, i.e. the transistors are operated as switches and not as linear amplifiers. The converter is assumed to be lossless, i.e. the conduction and switching losses of the switches of the converter legs are neglected for this analysis.

The switches in each leg operate complementary to each other. Also, leg A and leg B operate complementary to each other. This means that the upper switch of leg A and lower switch of leg B operate together and the lower switch of leg A and upper switch of leg B operate together. If u is the duty ratio of the upper switch in leg A and the lower switch in leg B, and T_s is the switching time period, then during this switching interval uT_s we get

$$v_A = v_s$$

$$v_B = 0$$

This results in a machine voltage of

$$v_m = v_A - v_B = v_s$$

During the remaining portion of the switching period $(1-u)T_s$, when the lower switch of leg A and the upper switch of leg B turn ON, we get

$$v_A = 0$$

$$v_B = v_s$$

and the resulting machine voltage is

$$v_m = v_A - v_B = -v_s$$

The average machine voltage during the complete switching period T_s is

$$\begin{aligned} v_m &= u\ v_s + (1-u)\ (-v_s) \\ &= (2u-1)v_s \end{aligned} \tag{1}$$

Since we assumed the converter to be lossless, we get the power balance equation between the input and output terminals of the converter as

$$v_s\ i_s = v_m\ i_a$$

From (1),

$$\begin{aligned} v_s\ i_s &= (2u-1)v_s i_a \\ \implies i_s &= (2u-1)i_a \end{aligned} \tag{2}$$

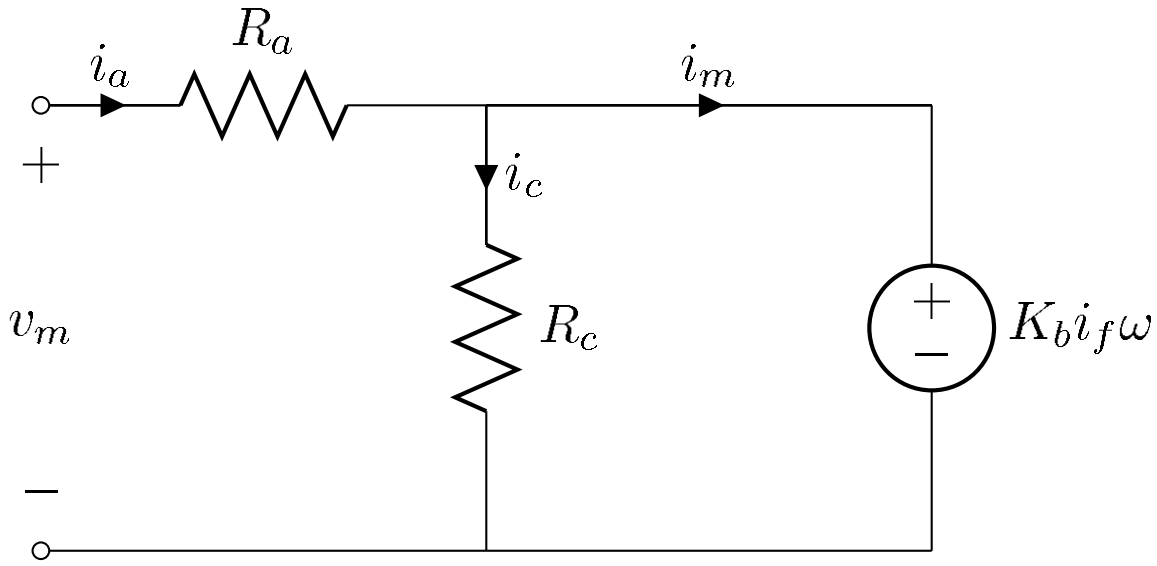

Figure 2: Steady-state equivalent circuit diagram of a DC machine (field circuit not shown).

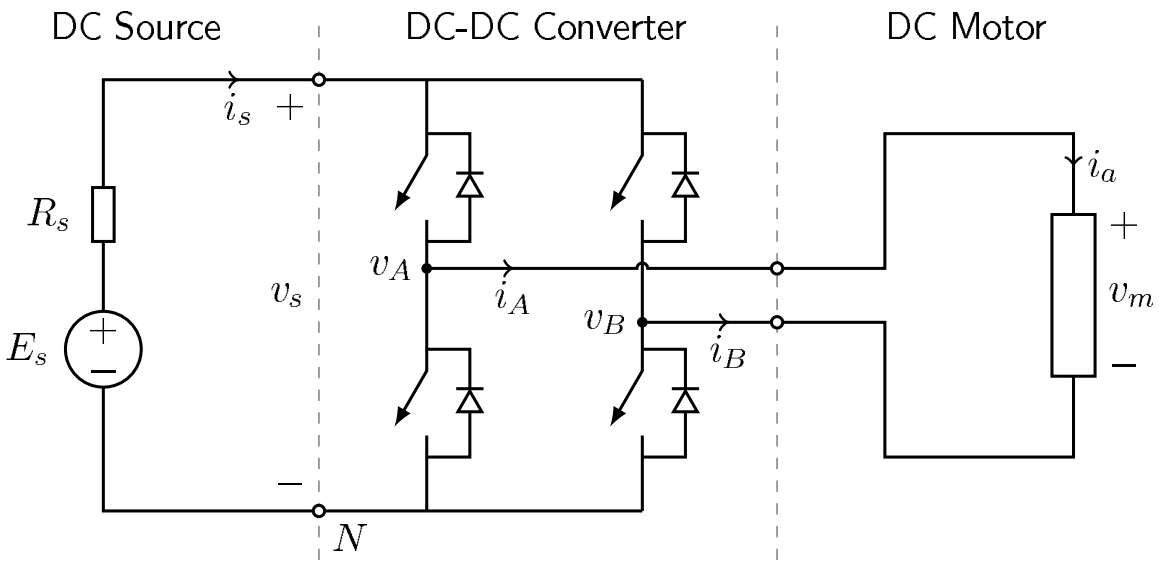

Figure 3: Schematic diagram showing the connection of the DC machine to the DC source through the DC-DC converter.

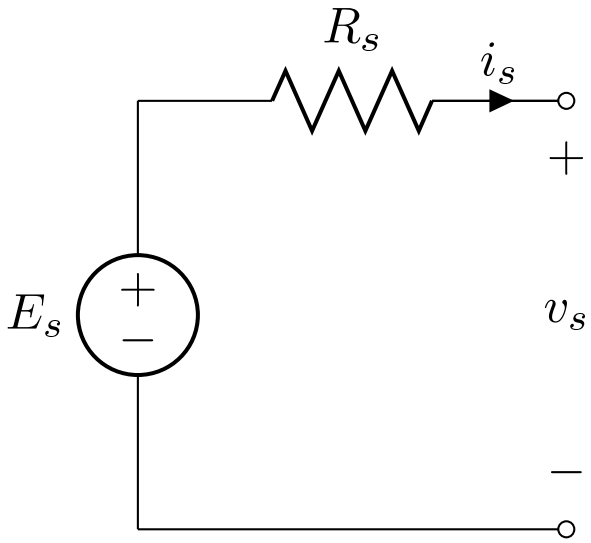

Figure 4: Steady-state equivalent circuit diagram of an electrochemical battery pack which is used as the DC source.

We can summarize the equations characterizing the equivalent circuit diagrams shown in Figure 2 and Figure 4, along with equations (1) and (2) as shown below. The field of the DC machine is assumed to be separately excited with the field flux within the saturation limit and its resistance has been neglected.

$$\begin{bmatrix} -R_c & R_c & 0 & 0 & 0 \\ R_c & -(R_a+R_c) & 1 & 0 & 0 \\ 0 & 0 & -1 & 0 & (2u-1) \\ 0 & (2u-1) & 0 & -1 & 0 \\ 0 & 0 & 0 & R_s & 1 \end{bmatrix} \begin{bmatrix} i_m \\ i_a \\ v_m \\ i_s \\ v_s \end{bmatrix} = \begin{bmatrix} K_b i_f \omega \\ 0 \\ 0 \\ 0 \\ E_s \end{bmatrix} \tag{3}$$

The electromagnetic torque equation of the machine is given by

$$T = K_b i_f i_m \tag{4}$$

2.2 Analysis

Forward motoring occurs within a feasible subset of the 1st-quadrant of the torque-speed plane where $T \geq 0$ and $\omega \geq 0$. Similarly, forward braking occurs within a feasible subset of the 4th-quadrant where $T \leq 0$ and $\omega \geq 0$. Regenerative braking occurs in a smaller feasible subset of the 4th-quadrant where $T \leq 0$, $\omega \geq 0$ and $i_s \leq 0$. We define the following optimization problems:

Problem 1: maximize torque, T

$$\text{subject to } (3)-(4),\ 0 \leq u \leq 1,\ |i_a| \leq I_{\max},\ 0 \leq i_f \leq I_{f\text{-max}},\ T \geq 0 \tag{5}$$

Problem 2: minimize torque, T

$$\text{subject to } (3)-(4),\ 0 \leq u \leq 1,\ |i_a| \leq I_{\max},\ 0 \leq i_f \leq I_{f\text{-max}},\ T \leq 0 \tag{6}$$

Problem 3: maximize torque, T

$$\text{subject to } (3)-(4),\ 0 \leq u \leq 1,\ |i_a| \leq I_{\max},\ 0 \leq i_f \leq I_{f\text{-max}},\ T \leq 0 \tag{7}$$

Problem 4: minimize torque, T

subject to $(3)-(4),\ 0 \le u \le 1,\ |i_a| \le I_{\max},\ 0 \le i_f \le I_{f\text{-max}},\ T \le 0,\ i_s \le 0$ (8)

Problem 5: maximize torque, T

subject to $(3)-(4),\ 0 \le u \le 1,\ |i_a| \le I_{\max},\ 0 \le i_f \le I_{f\text{-max}},\ T \le 0,\ i_s \le 0$ (9)

where $I_{\max}$ is the maximum input current given to the machine, $I_{f\text{-max}}$ is the maximum value of the field current. Problem 1 solves for the maximum motoring torque boundary in the 1st-quadrant. Problems 2 and 3 solve for the maximum and minimum braking torque boundaries in the 4th-quadrant. Problems 4 and 5 solve for the maximum and minimum regenerative braking torque boundaries in the 4th-quadrant. In addition to these, there is another optimization problem that is of interest:

Problem 6: minimize current, i_s

subject to $(3)-(4),\ 0 \le u \le 1,\ |i_a| \le I_{\max},\ 0 \le i_f \le I_{f\text{-max}},\ T \le 0,\ i_s \le 0$ (10)

Problem 6 solves for the maximum possible current that is transferred back to DC source during regenerative braking and associated with this solution is a corresponding regenerative braking torque.

2.3 Numerical Results

The above optimization problems were programmed into MATLAB and solved using the numerical optimization function `fmincon` of the Optimization Toolbox. The problems were solved for a separately excited DC machine and a permanent magnet DC machine.

2.3.1 Separately Excited DC Machine

The system parameters describing a separately excited DC machine are given below in Table 1. It should be noted that the field resistance has been neglected.

The solutions to the six optimization problems are plotted on the torque-speed plane as shown in Figure 5. It can be seen that the solution to Problem 4 divides

Table 1: Separately Excited DC Machine Parameters Used for Numerical Optimization

Parameter	**Value**
E_s	201.3 V
R_s	0.183 Ω
K_b	1.91 V/A-rads^{-1}
R_a	0.75 Ω
R_c	240 Ω
$I_{\max}$	20.0 A
$I_{f\text{-}\max}$	1.0 A
$\omega_{\max}$	1000 RPM

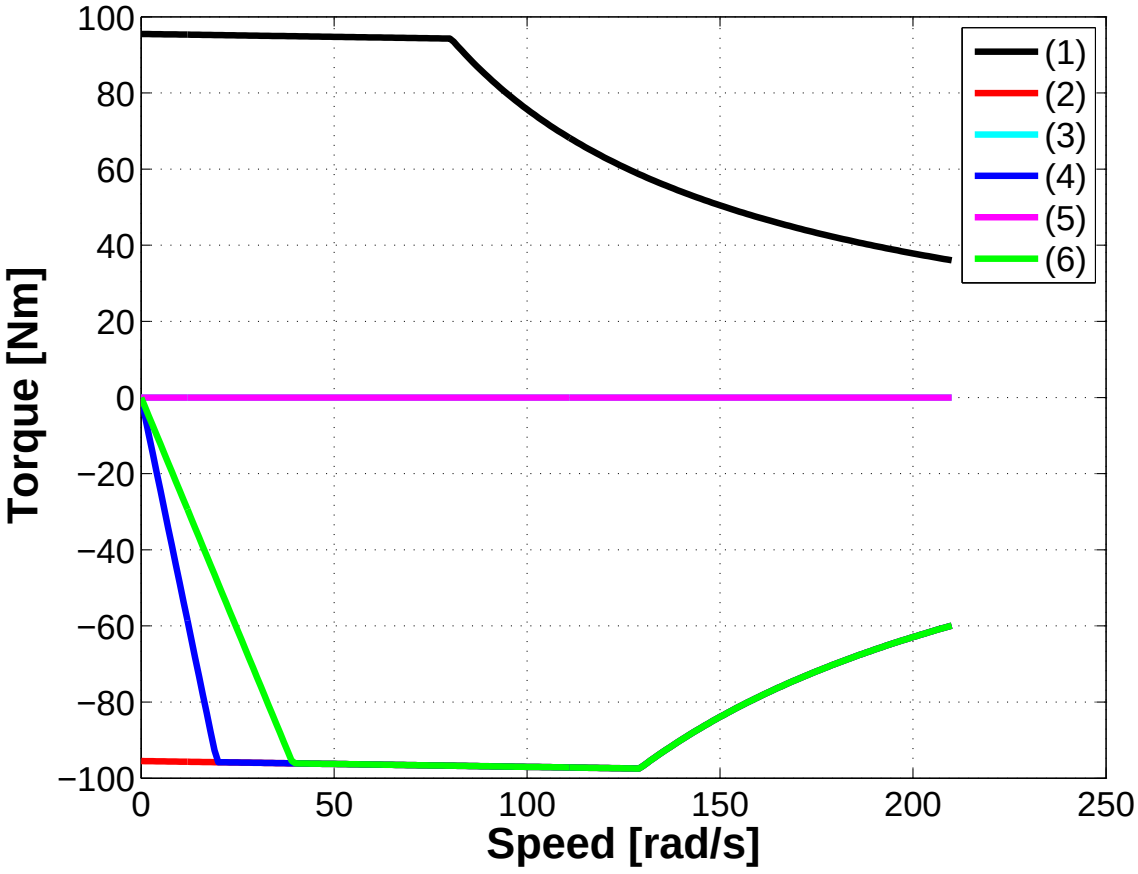

Figure 5: Numerical optimization solutions for seperately excited DC machine.

the forward braking quadrant into two sections. The section between the y axis and the solution to Problem 4 (shown in blue) represents the region of non-regenerative braking and the rest of the forward braking quadrant represents the region of regenerative braking. The solution to Problem 5 (shown in magenta) coincides with the x axis. This is due to the fact that the field current is supplied by an external circuit whose losses have not been considered while modeling the system. It can be seen that the solution to Problem 6 (shown in green) is a curve that passes through the origin in the braking quadrant. Operation along this line would result in maximum current absorbed by the DC source during regenerative braking.

2.3.2 Permanent Magnet DC Machine

The numerical optimization problems described earlier were also solved for a permanent magnet DC machine (PMDC). The magnetic field in the PMDC machine is supplied by permanent magnets that are attached to the stator of the machine. All of the above equations described for the separately excited DC machine remain unaltered except that the variable field current, i_f is replaced by a constant magnetic flux, Λ and a magnetic constant $K = K_b\Lambda$ is defined. This changes the back electromotive force (EMF) equation and electromagnetic torque in the following way:

$$\begin{aligned} E_m &= K\omega \\ T &= Ki_m \end{aligned} \tag{11}$$

The system parameters that describe the permanent magnet DC machine are listed below in Table 2 and its solutions are plotted as shown in Figure 6.

It can be seen that the torque-speed capability curve (shown in black and red) for the PMDC machine is quite different in its shape from that of the separately excited DC machine. This is due to the inability to perform flux weakening in the PMDC machine. Also, the solution to Problem 5 (shown in magenta) does not coincide with the x axis as earlier but is offset. Therefore, the solutions to Problems 4 (shown in

Table 2: Permanent Magnet DC Machine Parameters Used for Numerical Optimization

Parameter	Value
E_s	26.4 V
R_s	0.048 Ω
K	0.2 V/rads^{-1}
R_a	7.6 Ω
R_c	240 Ω
$I_{\max}$	2.0 A
$\omega_{\max}$	1500 RPM

blue) and 5 divide the forward braking quadrant into three sections. The sections close to x and y axes are the regions of non-regenerative braking and the middle section is the region of regenerative braking. The solution to Problem 6 (shown in green) represents the operation curve along which maximum current is sent back to the DC source through regenerative braking.

2.4 Symbolic Results

In this section, closed-form expressions describing the regenerative braking boundaries and the curve of maximum regenerative braking current are developed for a permanent magnet DC machine.

2.4.1 Neglecting Core Loss Resistance, R_c

In this section we consider the system of equations described in (3), and set R_c to infinity thereby allowing zero current to pass through it and the core-loss power $i_c^2 R_c$ becomes negligible.

2.4.1.1 Regenerative Braking Boundaries

The system is analyzed as follows. The DC source power is

$$P_s = E_s i_s \tag{12}$$

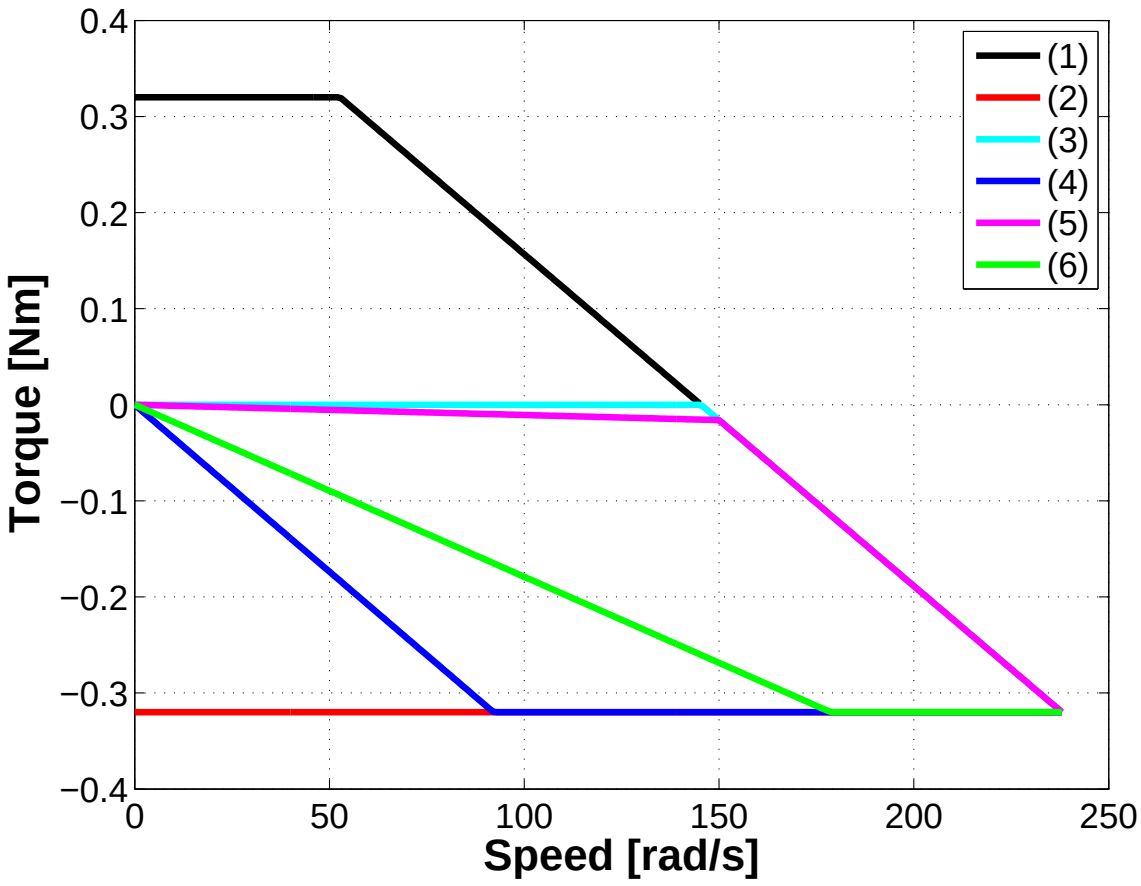

Figure 6: Numerical optimization solutions for permanent magnet DC machine.

The DC source power loss is

$$W_s = i_s^2 R_s$$

The electric machine input power is

$$P_e = v_m i_a$$

The electric machine output power is

$$P_m = T\omega \tag{13}$$

The electric machine power loss is

$$W_{em} = i_a^2 R_a$$

Since $i_c = 0$, we get $i_a = i_m$. The power balance equation on the machine side is

$$\begin{aligned} P_e &= P_m + W_{em} \\ &= T\omega + i_a^2 R_a \\ &= K i_m \omega + i_m^2 R_a \end{aligned} \tag{14}$$

The power balance equation on the DC source side is

$$\begin{aligned} P_s &= P_e + W_s \\ &= P_e + i_s^2 R_s \end{aligned}$$

Using (12), we get the source current as

$$i_s = \frac{E_s - \sqrt{E_s^2 - 4R_s P_e}}{2R_s} \tag{15}$$

To obtain the boundary between regenerative and non-regenerative braking, we set P_s to 0. This means power is neither removed nor absorbed from the DC source.

$$P_s = E_s i_s = 0$$

Since E_s is positive and non-zero

$$\implies i_s = 0$$

From (15), we get

$$\begin{aligned} \cancel{E_s^2} &= \cancel{E_s^2} - 4R_s P_e \\ \implies P_e &= 0 \end{aligned} \tag{16}$$

From (14), we get

$$\begin{aligned} K i_m \omega + i_m^2 R_a &= 0 \\ \implies i_m = -\left(\frac{K}{R_a}\right)\omega \ &\text{ and } \ i_m = 0 \end{aligned}$$

The electromagnetic torques corresponding to the above current expressions are

$$T = -\left(\frac{K^2}{R_a}\right)\omega \tag{17}$$

and

$$T = 0 \tag{18}$$

respectively.

The above torque expressions show that there are two boundaries that divide the regenerative and non-regenerative braking regions in the torque-speed plane in the absence of core-loss resistance, R_c. One boundary is a straight line in the 4th and 2nd quadrant, which passes through the origin with negative slope dependent on the machine's armature resistance, R_a, and magnetic constant, K, and the other is along the x-axis where $T = 0$, as shown in Figure 7. If the curve describing the regenerative braking boundary exceeds the boundaries of the torque-speed capability curve, the regenerative braking boundary follows the torque-speed capability curve. From (17) and (18) we can also conclude that inclusion of DC source resistance, R_s, does not affect the boundary between regenerative and non-regenerative operating regions in any way. However, it should be noted that R_s would affect the overall boundaries of the torque-speed capability curves.

2.4.1.2 Maximum Regenerative Braking Current

To obtain the expression for the maximum current absorbed by the DC source, we minimize the DC source current, i_s, with respect to the control current, i_a. From (15), we get

$$\frac{di_s}{di_a} = \frac{d}{di_a}\left(\frac{E_s - \sqrt{E_s^2 - 4R_sP_e}}{2R_s}\right) = 0$$

Since E_s and R_s are constant

$$\implies \frac{dP_e}{di_a} = 0 \tag{19}$$

Also since R_c is neglected, we have $i_a = i_m$.

$$\therefore \frac{dP_e}{di_a} = 0 \text{ is equivalent to } \frac{dP_e}{di_m} = 0$$

From (14), we get

$$\frac{dP_e}{di_m} = K\omega + 2R_a i_m = 0$$
$$\implies i_m = -\left(\frac{K}{2R_a}\right)\omega$$

The corresponding electromagnetic torque equation is

$$T = -\left(\frac{K^2}{2R_a}\right)\omega \tag{20}$$

The above torque expression is a straight line in the 4th and 2nd quadrants of the torque-speed plane and passes through the origin as shown in Figure 7. The slope of this line is negative and is half of that in (17). It can be observed that the source resistance, R_s, does not affect this expression as well. The maximum current absorbed by the source during regenerative braking is given as

$$i_{s,\text{max regen}} = \frac{E_s - \sqrt{E_s^2 + K^2\omega^2\left(\frac{R_s}{R_a}\right)}}{2R_s} \tag{21}$$

2.4.2 Including Core Loss Resistance, R_c

In this section, the effect of core loss resistance, R_c, on the regenerative braking boundaries is examined for a permanent magnet DC machine. The curves describing the regenerative braking boundaries and the curve of maximum regenerative braking current are obtained as follows.

2.4.2.1 Regenerative Braking Boundaries

Using the equations in (3), we can write the following equations. The electric machine core loss power is given by

$$W_{Fe} = (i_a - i_m)^2 R_c$$

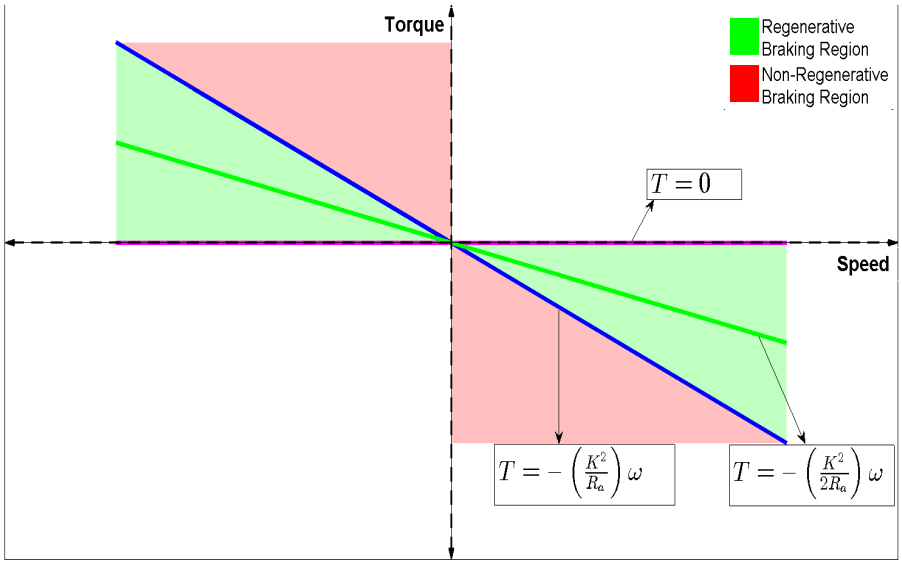

Figure 7: Regenerative braking boundaries and maximum regenerative braking current curve for a permanent magnet DC machine neglecting core loss resistance, R_c.

The total electric machine power loss, which is the sum of both copper loss and core loss, is written as

$$W_{em} = i_a^2 R_a + (i_a - i_m)^2 R_c$$

Using (13), we get the power balance equation for the machine as

$$\begin{aligned} P_e &= P_m + W_{em} \\ &= T\omega + i_a^2 R_a + (i_a - i_m)^2 R_c \end{aligned}$$

From (3) and (11), we have

$$i_a = i_m + \frac{K\omega}{R_c} \quad \text{and} \quad T = K i_m$$

$$\implies P_e = K i_m \omega + \left(i_m + \frac{K\omega}{R_c}\right)^2 R_a + \frac{K^2\omega^2}{R_c}$$

Defining $\gamma = \dfrac{R_a}{R_c}$, we get

$$P_e = i_m^2 R_a + K\omega(1 + 2\gamma) i_m + \frac{K^2\omega^2}{R_c}(1 + \gamma)$$

Following the results obtained in (16), we set $P_e = 0$

$$P_e = i_m^2 R_a + K\omega(1+2\gamma)i_m + \frac{K^2\omega^2}{R_c}(1+\gamma) = 0 \tag{22}$$

Solving for i_m, we get

$$i_m = -\left(\frac{K(1+\gamma)}{R_a}\right)\omega \text{ and } i_m = -\left(\frac{K\gamma}{R_a}\right)\omega$$

The corresponding electromagnetic torques associated with above currents are

$$T = -\left(\frac{K^2(1+\gamma)}{R_a}\right)\omega \tag{23}$$

and

$$T = -\left(\frac{K^2\gamma}{R_a}\right)\omega \tag{24}$$

respectively.

When the expressions for torque in (23) and (24) are plotted on the torque-speed plane, two straight lines with negative slopes and passing through the origin are obtained. These curves divide the braking quadrants (4th and 2nd) each into three sections. The two sections adjacent to the axes are non-regenerative braking regions and the center section corresponds to the region of regenerative braking as shown in Figure 8.

2.4.2.2 Maximum Regenerative Braking Current

In order to determine the maximum power absorbed by the DC source, we again use the concept of minimizing the DC source current, i_s, with respect to control current i_a. From (19), we have

$$\frac{di_s}{di_a} = 0 \text{ is equivalent to } \frac{dP_e}{di_a} = 0$$

$$\frac{dP_e}{di_a} = \frac{dP_e}{di_m} \cdot \frac{di_m}{di_a} = 0$$

Since $i_a = i_m + \dfrac{K\omega}{R_c}$, we have

$$\frac{di_m}{di_a} = 1$$

Using the expression for P_e from (22), we get

$$\frac{dP_e}{di_a} = \frac{dP_e}{di_m} = 2R_a i_m + K\omega(1+2\gamma) = 0$$
$$\therefore \quad i_m = -\left(\frac{K(1+2\gamma)}{2R_a}\right)\omega$$

The electromagnetic torque corresponding to this current is

$$T = -\left(\frac{K^2(1+2\gamma)}{2R_a}\right)\omega \tag{25}$$

Substituting this value of torque in (22), we get

$$P_e = -\left(\frac{K^2}{4R_a}\right)\omega^2$$

Finally, substituting this value of P_e in (15), we get the DC source current as

$$i_{s,\text{max regen}} = \frac{E_s - \sqrt{E_s^2 + K^2\omega^2\left(\dfrac{R_s}{R_a}\right)}}{2R_s} \tag{26}$$

It can be observed that the expression obtained for maximum recharge current while including core loss resistance, shown in (26), is identical to that obtained in the previous section where core loss resistance was neglected, as shown in (21). When the expression for torque obtained in (25) is plotted on the torque-speed plane, we get a straight line passing through the origin with negative slope in the 4th and 2nd quadrant as shown in Figure 8.

The curves representing the torque expressions in (23), (24) and (25) are identical to that of the numerical solutions for Problem 4, Problem 5 and Problem 6 respectively, for the permanent magnet DC machine as shown in Figure 6. The curves match each other until the numerical values of the symbolic expressions exceed the torque-speed capability boundary beyond which they are forced to merge with torque-speed capability boundary for the rest of the speed range.

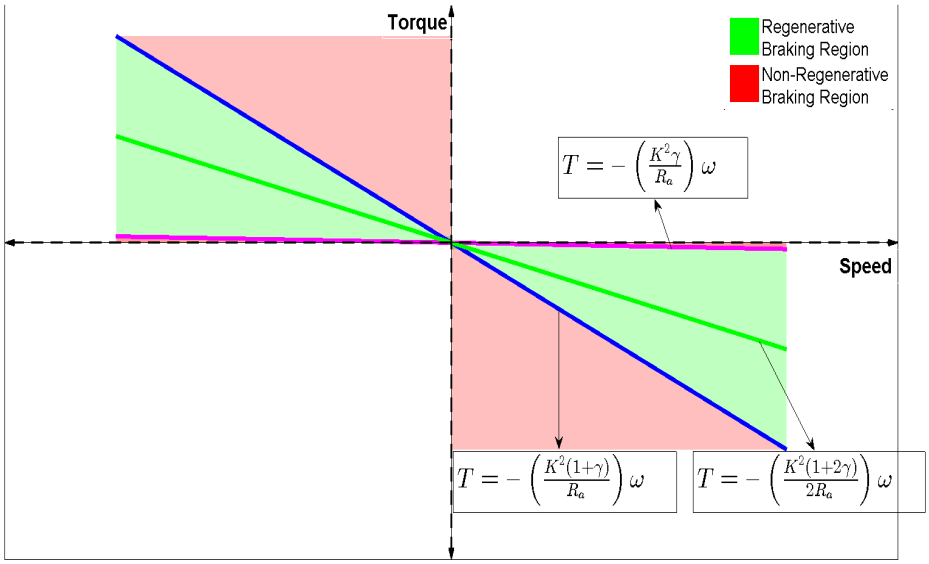

Figure 8: Regenerative braking boundaries and maximum regenerative braking current curve for a permanent magnet DC machine including core loss resistance, R_c.

Therefore, we have developed closed-form expressions describing the boundaries of regenerative braking and the maximum current absorbed by the DC source during regenerative braking, in the context of a permanent magnet DC machine. This analysis provides a better understanding of the dependence of regenerative braking boundaries and maximum regenerative braking current curve on the machine parameters.

CHAPTER III

REGENERATIVE BRAKING IN PERMANENT MAGNET SYNCHRONOUS MACHINES

3.1 Modeling

The cross-section geometry of a two-pole interior-permanent-magnet three-phase synchronous machine is shown in Figure 9, where θ denotes the rotor position and stator *abc* axes and rotor *dq* axes are displayed. The three stator phase windings are assumed to be star-connected and are connected to the midpoints of the three legs of a controllable DC-AC power converter as shown in Figure 10. The DC-AC converter (inverter) consists of three identical legs consisting of two switches and two diodes each. The control terminal of each switch is not shown. Each leg of the inverter is operated with a pulse width modulated switch duty ratio to produce a balanced three-phase output which is given as the input to the electric machine. Both of the switches in the same leg cannot be turned ON at the same time, as it would short the input voltage. Thus the nature of operation of the two switches in the same leg is complementary.

The DC-side of the power converter is connected to a DC power source (an electrochemical battery pack) with bus capacitance. The steady-state equivalent circuit diagram of the electrochemical battery pack is the same as that seen earlier in Figure 4. The storage system variables are denoted by subscript s, the DC-AC converter circuit variables by subscripts ABC and the machine phase variables by subscripts *abc*. The key idea is to project stator voltages and stator currents onto a $dq0$ reference frame that rotates with the rotor, and further to reduce the number of voltage and current co-ordinates from three to two by exploiting the property of symmetrical

and balanced phase windings. The $dq0$ representations of the abc phase variables are defined by

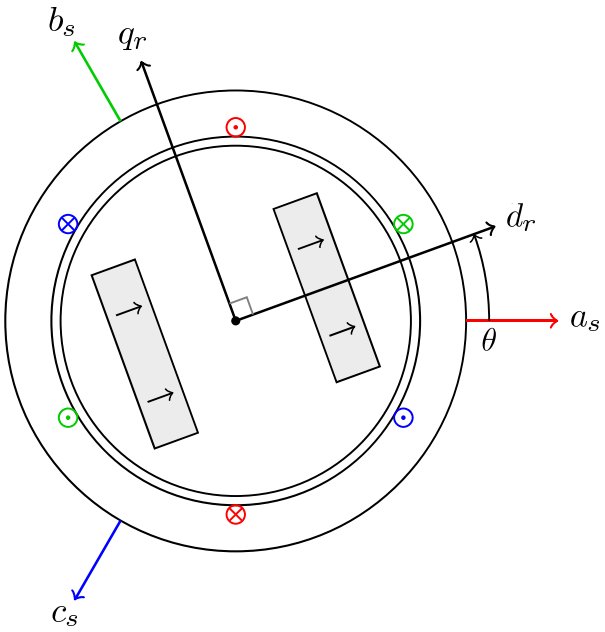

Figure 9: Cross-section of a two pole interior permanent magnet synchronous machine.

$$\begin{bmatrix} v_d \\ v_q \\ v_0 \end{bmatrix} = \sqrt{\frac{2}{3}} \begin{bmatrix} \cos(N\theta) & \cos(N\theta - \frac{2}{3}\pi) & \cos(N\theta + \frac{2}{3}\pi) \\ -\sin(N\theta) & -\sin(N\theta - \frac{2}{3}\pi) & -\sin(N\theta + \frac{2}{3}\pi) \\ \frac{1}{\sqrt{2}} & \frac{1}{\sqrt{2}} & \frac{1}{\sqrt{2}} \end{bmatrix} \begin{bmatrix} v_a \\ v_b \\ v_c \end{bmatrix}$$

$$\begin{bmatrix} i_d \\ i_q \\ i_0 \end{bmatrix} = \sqrt{\frac{2}{3}} \begin{bmatrix} \cos(N\theta) & \cos(N\theta - \frac{2}{3}\pi) & \cos(N\theta + \frac{2}{3}\pi) \\ -\sin(N\theta) & -\sin(N\theta - \frac{2}{3}\pi) & -\sin(N\theta + \frac{2}{3}\pi) \\ \frac{1}{\sqrt{2}} & \frac{1}{\sqrt{2}} & \frac{1}{\sqrt{2}} \end{bmatrix} \begin{bmatrix} i_a \\ i_b \\ i_c \end{bmatrix}$$

where N is the number of pole-pairs of the machine. Analysis shows that $v_0 \equiv 0$ and $i_0 \equiv 0$, hence only the dq variables will be considered.

The steady-state physics of the electric machine are indicated by the equivalent d-axis and q-axis circuit diagrams shown in Figure 11 as described in [10]. The phase voltages in the d and q axes are represented as v_d and v_q, the phase currents are i_d and

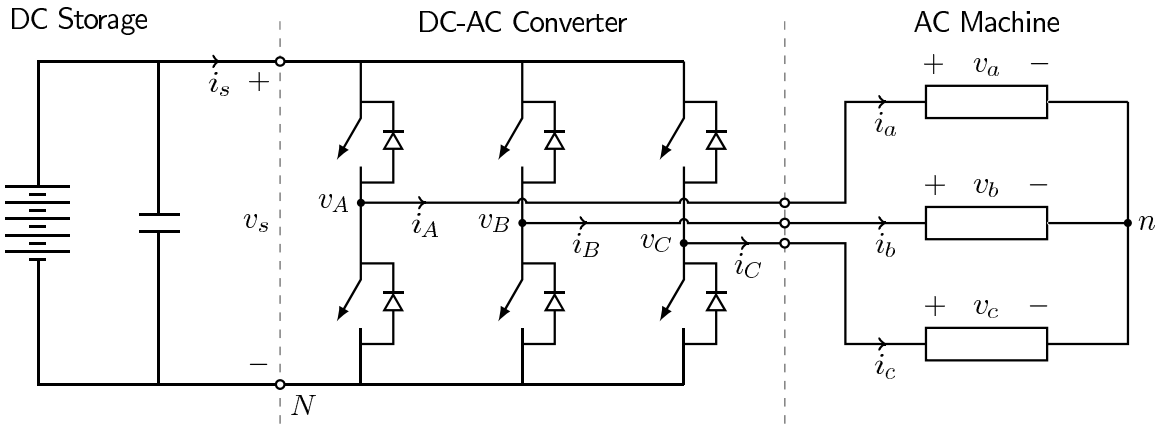

Figure 10: Schematic of a star-connected AC machine connected to the DC source through a DC-AC converter.

i_q and the magnetizing components of the currents are i_{dm} and i_{qm} respectively. The electric machine phase resistance and iron-loss resistance are R_p and R_c, respectively; its inductances are L_d and L_q, the permanent-magnet flux is Λ and the rotor speed is ω.

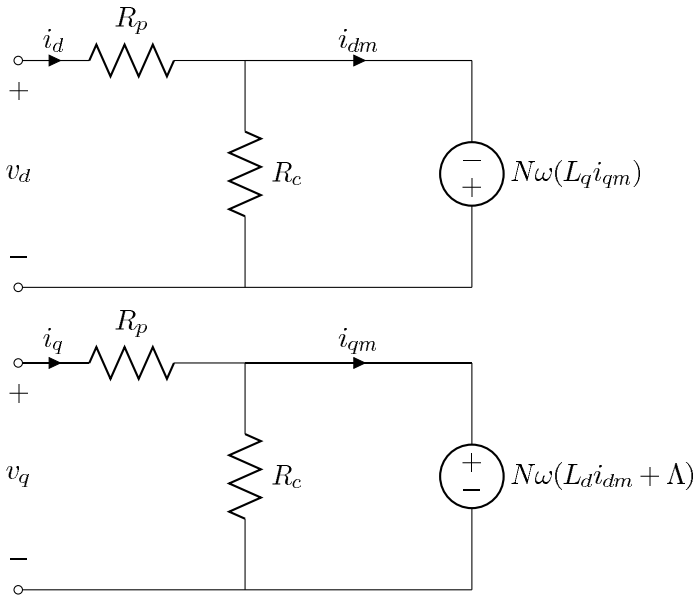

Figure 11: Steady-state equivalent circuit models in the d and q axes of an interior-permanent-magnet synchronous machine.

The relationship between phase voltages v_{abc} and converter leg voltages v_{ABC} will

be established based on Figure 10 as follows.

$$\begin{bmatrix} v_A \\ v_B \\ v_C \end{bmatrix} = \begin{bmatrix} \text{voltage at terminal } A \text{ with respect to node } N \\ \text{voltage at terminal } B \text{ with respect to node } N \\ \text{voltage at terminal } C \text{ with respect to node } N \end{bmatrix}$$

Applying KVL along converter leg voltages, motor phase voltages and v_{nN}, the voltage of node n with respect to N, we get

$$\begin{bmatrix} v_a \\ v_b \\ v_c \end{bmatrix} = \begin{bmatrix} v_A - v_{nN} \\ v_B - v_{nN} \\ v_C - v_{nN} \end{bmatrix}$$

Adding these three equations and combining it with the fact that $v_a + v_b + v_c = 0$, we get

$$v_{nN} = \frac{1}{3}(v_A + v_B + v_C)$$

$$\therefore \begin{bmatrix} v_a \\ v_b \\ v_c \end{bmatrix} = \frac{1}{3} \begin{bmatrix} 2 & -1 & -1 \\ -1 & 2 & -1 \\ -1 & -1 & 2 \end{bmatrix} \begin{bmatrix} v_A \\ v_B \\ v_C \end{bmatrix}$$

If u_A, u_B and u_C represent the duty-cycle commands of the three converter legs and v_s represents the DC voltage on the DC-side of the DC-AC converter, then

$$\begin{bmatrix} v_A \\ v_B \\ v_C \end{bmatrix} = \begin{bmatrix} u_A \\ u_B \\ u_C \end{bmatrix} v_s$$

If we use the simplest form of duty-cycle assignment

$$\begin{bmatrix} u_A \\ u_B \\ u_C \end{bmatrix} = \frac{1}{2} + \frac{v_{ref}}{v_s} \begin{bmatrix} \cos(N\theta + \phi_v) \\ \cos(N\theta - \frac{2}{3}\pi + \phi_v) \\ \cos(N\theta + \frac{2}{3}\pi + \phi_v) \end{bmatrix}$$

where v_{ref} is the reference voltage and ϕ_v is the converter phase angle, this would result in the $dq0$ voltages being

$$\begin{bmatrix} v_d \\ v_q \\ v_0 \end{bmatrix} = \sqrt{\frac{3}{2}} v_{ref} \begin{bmatrix} \cos\phi_v \\ \sin\phi_v \\ 0 \end{bmatrix}$$

The fact that $v_0 = 0$ follows directly from the phasor addition theorem. This establishes the connection between the sinusoidal converter leg voltages imposed by control and the resulting constant motor phase voltage vector in the dq frame of reference. We can define u_d and u_q to be the duty-cycles of the DC-AC converter in the dq reference frame. Then

$$\begin{bmatrix} u_d \\ u_q \end{bmatrix} = \sqrt{\frac{3}{2}} \left(\frac{v_{ref}}{v_s} \right) \begin{bmatrix} \cos\phi_v \\ \sin\phi_v \end{bmatrix} \tag{27}$$

From (27), we can rewrite the dq phase voltages as

$$\begin{bmatrix} v_d \\ v_q \end{bmatrix} = \begin{bmatrix} u_d \\ u_q \end{bmatrix} v_s \tag{28}$$

The magnitude of the converter duty-cycles vector in the dq plane is given as

$$U_{dq} = ||u_{dq}|| = \sqrt{u_d^2 + u_q^2} = \sqrt{\frac{3}{2}} \left(\frac{v_{ref}}{v_s} \right) \tag{29}$$

The schematic diagram shows that the converter leg voltages are constrained by

$$0 \leq v_A \leq v_s$$

$$0 \leq v_B \leq v_s$$

$$0 \leq v_C \leq v_s$$

Using the expression for duty cycles, it follows that

$$0 \leq v_{ref} \leq \frac{1}{2} v_s$$

$$\therefore \ \max(v_{ref}) = \frac{1}{2} v_s$$

From (29),

$$\implies \max(U_{dq}) = \frac{1}{2}\sqrt{\frac{3}{2}} \tag{30}$$

If we define the converter duty-cycles, u_A, u_B and u_C to include third-harmonic injection, we get

$$\begin{bmatrix} u_A \\ u_B \\ u_C \end{bmatrix} = \frac{1}{2} + \frac{v_{ref}}{v_s} \left(\begin{bmatrix} \cos(N\theta + \phi_v) \\ \cos(N\theta - \frac{2}{3}\pi + \phi_v) \\ \cos(N\theta + \frac{2}{3}\pi + \phi_v) \end{bmatrix} - \frac{1}{6} \begin{bmatrix} \cos(3(N\theta + \phi_v)) \\ \cos(3(N\theta - \frac{2}{3}\pi + \phi_v)) \\ \cos(3(N\theta + \frac{2}{3}\pi + \phi_v)) \end{bmatrix} \right)$$

It can be shown that the equations for dq phase voltages, dq converter duty cycles obtained in (27) remain unchanged. However, as described in [11] the maximum value of v_{ref} changes to

$$0 \leq v_{ref} \leq \frac{1}{\sqrt{3}} v_s$$
$$\therefore \max(v_{ref}) = \frac{1}{\sqrt{3}} v_s$$

From (29),

$$\implies \max(U_{dq}) = \frac{1}{\sqrt{2}} \tag{31}$$

It can be observed that the maximum length of the duty-cycle vector, U_{dq}, depends on the pulse-width modulation technique used. For a star-connected electric machine, the maximum length of the machine phase voltage vector using PWM without 3rd-harmonic injection is

$$\max(V_{dq}) = \max(|| \langle v_d, v_q \rangle ||) = \frac{1}{2}\sqrt{\frac{3}{2}} v_s$$

and using PWM with 3rd-harmonic injection is

$$\max(V_{dq}) = \max(|| \langle v_d, v_q \rangle ||) = \frac{1}{\sqrt{2}} v_s$$

For a delta-connected machine, it can be shown that the maximum length of the machine phase voltage vector using PWM without 3rd-harmonic injection is

$$\max(V_{dq}) = \max(||\langle v_d, v_q \rangle||) = \frac{3}{2\sqrt{2}} v_s$$

and using PWM with 3rd-harmonic injection,

$$\max(V_{dq}) = \max(||\langle v_d, v_q \rangle||) = \frac{3}{\sqrt{2}} v_s$$

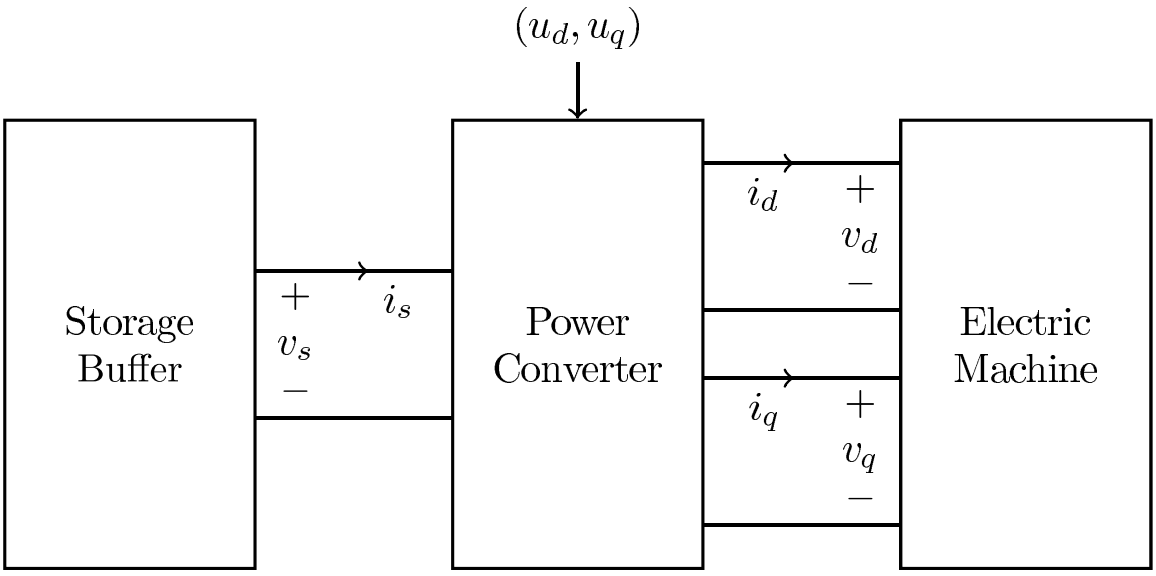

Figure 12: Abstracted block diagram of the DC source, DC-AC power converter and electric machine in terms of d and q variables in the rotor frame of reference.

Figure 12 shows an abstracted view of the DC source, DC-AC power converter and electric machine in terms of rotor-frame variables denoted by subscripts dq with u_d and u_q applied to the DC-AC power converter. From Figure 12, the following power balance equations can be written. The electric machine input power is

$$P_e = v_a i_a + v_b i_b + v_c i_c = v_d i_d + v_q i_q \tag{32}$$

Assuming lossless connections between the electric machine and the DC-AC converter, we get

$$v_A i_A + v_B i_B + v_C i_C = v_d i_d + v_q i_q$$

Since we assumed the DC-AC converter to be lossless, we get the power balance equation as

$$\begin{aligned} v_s i_s &= v_A i_A + v_B i_B + v_C i_C \\ &= v_d i_d + v_q i_q \\ \implies i_s &= \frac{v_d}{v_s} i_d + \frac{v_q}{v_s} i_q \end{aligned}$$

Using (28), we obtain

$$i_s = u_d i_d + u_q i_q \tag{33}$$

The internal resistance of the battery is R_s, and its open-circuit voltage is E_s, which is the same as that discussed in Chapter 2. According to Figure 4, Figure 11 and the equations 28 and 33 derived above, the model of the motor-generator unit may be expressed in the form

$$\begin{bmatrix} -R_c & 0 & R_p+R_c & 0 & -1 & 0 & 0 & 0 \\ 0 & -R_c & 0 & R_p+R_c & 0 & -1 & 0 & 0 \\ R_c & -N\omega L_q & -R_c & 0 & 0 & 0 & 0 & 0 \\ N\omega L_d & R_c & 0 & -R_c & 0 & 0 & 0 & 0 \\ 0 & 0 & 0 & 0 & -1 & 0 & 0 & u_d \\ 0 & 0 & 0 & 0 & 0 & -1 & 0 & u_q \\ 0 & 0 & u_d & u_q & 0 & 0 & -1 & 0 \\ 0 & 0 & 0 & 0 & 0 & 0 & R_s & 1 \end{bmatrix} \begin{bmatrix} i_{dm} \\ i_{qm} \\ i_d \\ i_q \\ v_d \\ v_q \\ i_s \\ v_s \end{bmatrix} = \begin{bmatrix} 0 \\ 0 \\ 0 \\ -N\omega\Lambda \\ 0 \\ 0 \\ 0 \\ E_s \end{bmatrix} \tag{34}$$

The electromagnetic torque is

$$T = N(\Lambda + (L_d - L_q) i_{dm}) i_{qm} \tag{35}$$

3.2 Analysis

As discussed earlier in Section 2.2, in order to determine the torque-speed boundaries of motoring, braking and regenerative braking, the following optimization problems

are defined.

Problem 1: maximize torque, T

$$\text{subject to } (34)-(35),\ ||u_{dq}|| \leq \max(U_{dq}),\ ||i_{dq}|| \leq I_{\max},\ T \geq 0 \tag{36}$$

Problem 2: minimize torque, T

$$\text{subject to } (34)-(35),\ ||u_{dq}|| \leq \max(U_{dq}),\ ||i_{dq}|| \leq I_{\max},\ T \leq 0 \tag{37}$$

Problem 3: maximize torque, T

$$\text{subject to } (34)-(35),\ ||u_{dq}|| \leq \max(U_{dq}),\ ||i_{dq}|| \leq I_{\max},\ T \leq 0 \tag{38}$$

Problem 4: minimize torque, T

$$\text{subject to } (34)-(35),\ ||u_{dq}|| \leq \max(U_{dq}),\ ||i_{dq}|| \leq I_{\max},\ T \leq 0,\ i_s \leq 0 \tag{39}$$

Problem 5: maximize torque, T

$$\text{subject to } (34)-(35),\ ||u_{dq}|| \leq \max(U_{dq}),\ ||i_{dq}|| \leq I_{\max},\ T \leq 0,\ i_s \leq 0 \tag{40}$$

Problem 6: minimize current, i_s

$$\text{subject to } (34)-(35),\ ||u_{dq}|| \leq \max(U_{dq}),\ ||i_{dq}|| \leq I_{\max},\ T \leq 0,\ i_s \leq 0 \tag{41}$$

where $\max(U_{dq})$ is the maximum assignable length of the duty-cycle vector U_{dq} which depends on the PWM technique, and $I_{\max}$ is the maximum permissible length of the current vector i_{dq}. Problem 1 solves for the maximum motoring torque boundary in the 1st-quadrant. Problems 2 and 3 solve for the maximum and minimum braking torque boundaries in the 4th-quadrant. Problems 4 and 5 solve for the maximum and minimum regenerative braking torque boundaries in the 4th-quadrant. Problem 6 solves for the maximum possible current that is transferred back to DC source during regenerative braking and associated with this solution is a corresponding regenerative braking torque.

3.3 Numerical Results

The above optimization problems were programmed into MATLAB and solved using the numerical optimization function `fmincon` found in the Optimization Toolbox.

The parameters of two different interior permanent magnet synchronous machines were considered and used to solve the optimization problems, denoted as IPM-A and IPM-B. The parameters of a surface-mounted permanent magnet synchronous machine were also used to solve the optimization problems.

3.3.1 IPM-A

Table 3: Interior Permanent Magnet Synchronous Machine (Star-Connected) Parameters Used for Numerical Optimization (IPM-A)

Parameter	**Value**
E_s	366.3 V
R_s	0.0247 Ω
N	4
R_p	0.297 Ω
R_c	240 Ω
L_d	0.5841 mH
L_q	0.6039 mH
Λ	0.2350 Wb
$I_{\max}$	300 A
$\max(U_{dq})$	$\frac{1}{\sqrt{2}}$
$\omega_{\max}$	10000 RPM

The solutions to the six optimization problems for IPM-A are plotted on the torque-speed plane as shown in Figure 13. It can be seen that the solutions to Problems 4 and 5 (shown in blue and magenta) divide the forward braking quadrant into three sections. The sections close to the x and y axes represent regions of non-regenerative braking and the middle section represents the region of regenerative braking. It can be seen that the solution to Problem 6 (shown in green) is a curve passing through the origin in the forward braking quadrant. Operation along this line would result in maximum current absorbed by the DC source during regenerative braking.

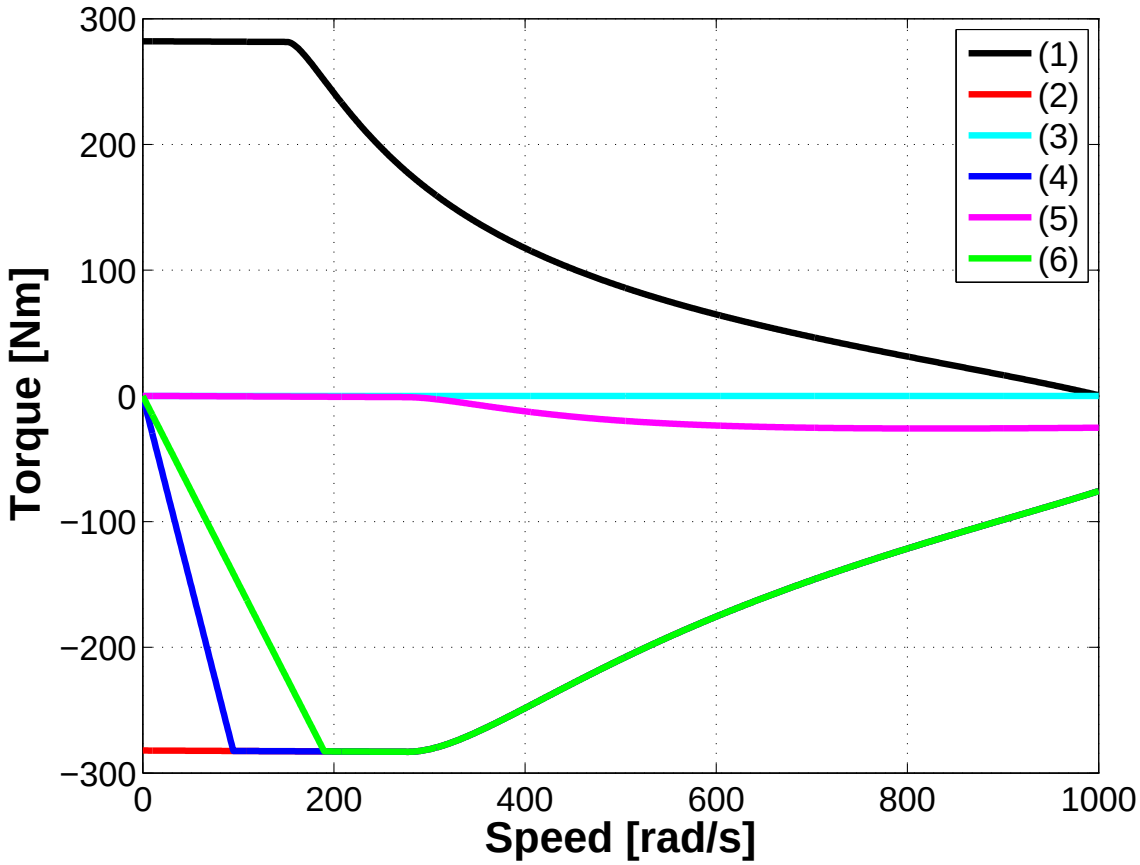

Figure 13: Numerical optimization solutions of the interior permanent magnet synchronous machine IPM-A.

Table 4: Interior Permanent Magnet Synchronous Machine (Star-Connected) Parameters Used for Numerical Optimization (IPM-B)

Parameter	**Value**
E_s	402.6 V
R_s	0.0366 Ω
N	4
R_p	0.57 Ω
R_c	240 Ω
L_d	3 mH
L_q	5 mH
Λ	0.2 Wb
$I_{\max}$	250 A
$\max(U_{dq})$	$\frac{1}{\sqrt{2}}$
$\omega_{\max}$	10000 RPM

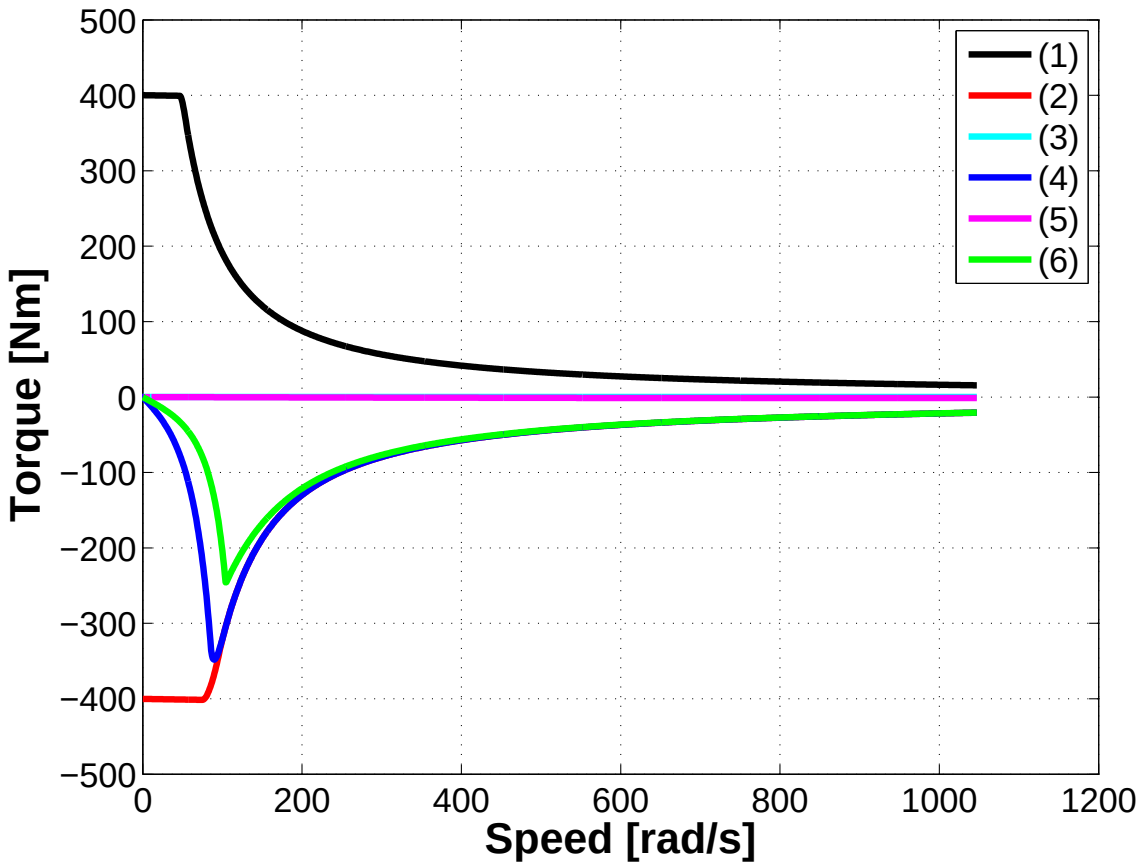

Figure 14: Numerical optimization solutions of the interior permanent magnet synchronous machine IPM-B.

3.3.2 IPM-B

From Figure 14 it can be seen that the solutions to Problems 4 and 5 (shown in blue and magenta) for IPM-B also divide the braking quadrant into three regions. However, the shape of the curve describing the solution to Problem 4 is different from that of IPM-A which is shown in Figure 13. Similarly, the shape of the curve describing the solution to Problem 6 (shown in green) is also different from that of IPM-A. This is attributed to the difference in machine parameters since all of the equations describing the system, the optimization problems and solution method remain the same.

3.3.3 SPM

The surface permanent magnet (SPM) synchronous machine is a special case of permanent magnet synchronous machines. All of the above equations described for the interior permanent magnet synchronous machine remain unaltered except that $L_d = L_q = L$. Using this condition, the torque equation shown in (35) reduces to

$$T = N\Lambda i_{qm} \tag{42}$$

The system parameters describing the surface permanent magnet synchronous machine are listed below in Table 5 and the solutions to the optimization problems are plotted as shown in Figure 15.

Table 5: Surface Permanent Magnet Synchronous Machine (Delta-Connected) Parameters Used for Numerical Optimization

Parameter	**Value**
E_s	26.4 V
R_s	0.048 Ω
N	4
R_p	1.2 Ω
R_c	150 Ω
$L_d = L_q = L$	1.8 mH
Λ	0.011 Wb
$I_{\max}$	2.5 A
$\max(U_{dq})$	$\frac{3}{2\sqrt{2}}$
$\omega_{\max}$	9000 RPM

It can be seen that the solutions to Problems 4 and 5 (shown in blue and magenta) divide the forward braking quadrant into regions of regenerative and non-regenerative braking here as well. Also, the solution to Problem 6 (shown in green) is a curve in the forward braking quadrant that passes through the origin.

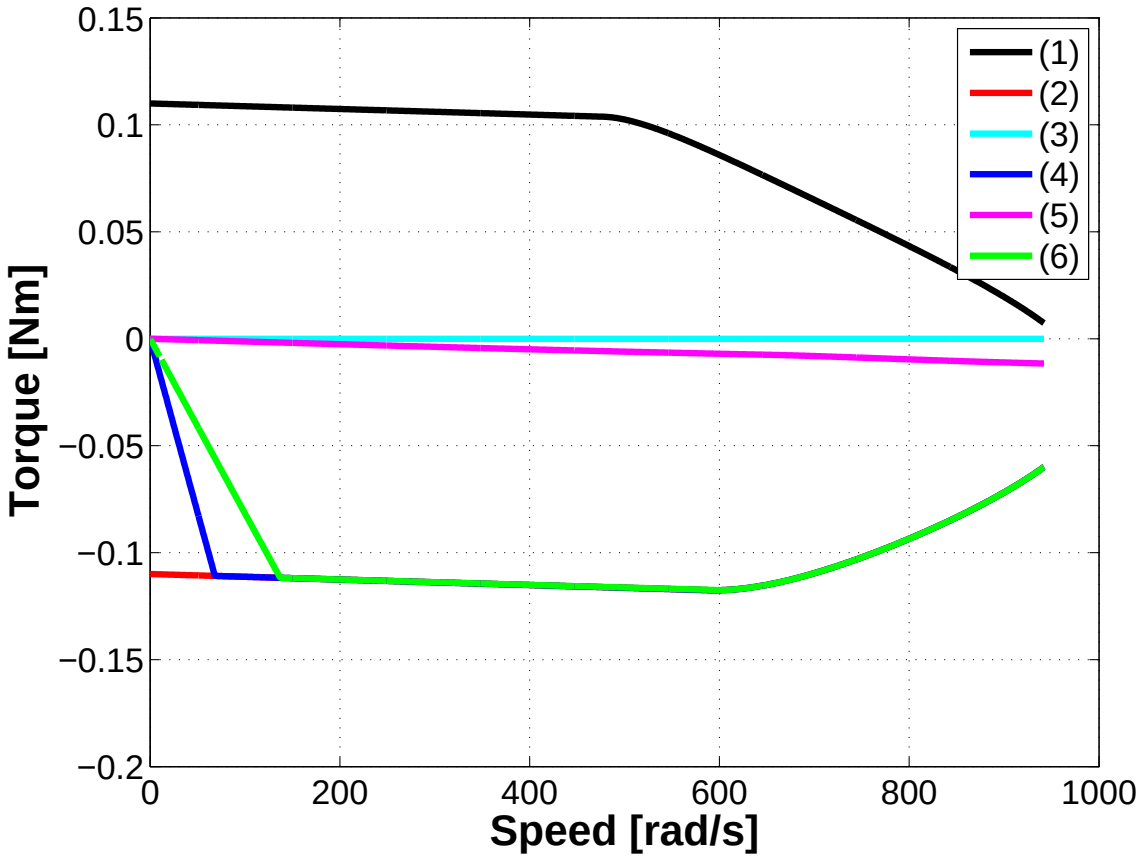

Figure 15: Numerical optimization solutions of the surface permanent magnet synchronous machine.

3.4 Symbolic Results

In order to understand the effects of the system parameters on the regenerative braking boundaries, the surface mounted permanent magnet synchronous machine with and without core loss resistance, R_c, is studied.

3.4.1 Neglecting Core Loss Resistance, R_c

As discussed earlier in the DC machine section, the current in the core loss path is considered to be zero, i.e $i_d = i_{dm}$ and $i_q = i_{qm}$. Therefore, the core loss power is negligible. The expressions describing the regenerative braking boundaries and maximum regenerative braking current are obtained as follows.

3.4.1.1 Regenerative Braking Boundaries

The electric machine power loss is given as

$$W_{em} = (i_d^2 + i_q^2)R_p$$

The electric machine output power is

$$P_m = T\omega$$

From (42) and using $i_q = i_{qm}$, we get

$$P_m = N\Lambda i_q \omega$$

From (32), the electric machine input power is

$$P_e = v_d i_d + v_q i_q$$

Using the above expressions, the following power balance equation can be written

$$\begin{aligned} P_e &= P_m + W_{em} \\ &= N\Lambda i_q \omega + (i_d^2 + i_q^2)R_p \end{aligned}$$

As seen in the DC machine section earlier, the regenerative braking boundary is obtained by setting $P_e = 0$. However, there are two control variables in this case, i_d and i_q. Using the equality constraint $P_e = 0$, we get i_q in terms of i_d as

$$i_q = \frac{-N\Lambda\omega \pm \sqrt{N^2\Lambda^2\omega^2 - 4R_p^2 i_d^2}}{2R_p} \tag{43}$$

The torque expression is given as

$$\begin{aligned} T &= N\Lambda i_q \\ &= N\Lambda \left(\frac{-N\Lambda\omega \pm \sqrt{N^2\Lambda^2\omega^2 - 4R_p^2 i_d^2}}{2R_p} \right) \end{aligned}$$

Therefore, it can be seen that by using the equality constraint the torque expression is dependent on only one control variable, i.e. i_d. Since we are finding the maximum and minimum braking torque that can be produced while obeying the equality constraint $P_e = 0$, we find the gradient of the torque expression with respect to the control variable i_d and set it equal to zero. We get

$$\begin{aligned} \frac{dT}{di_d} &= 0 \\ \implies i_d &= 0 \end{aligned}$$

Using this expression for i_d in (43), we get

$$i_q = -\left(\frac{N\Lambda}{R_p}\right)\omega \;\text{ and }\; i_q = 0$$

The electromagnetic torques corresponding to the above currents are

$$T = -\left(\frac{N^2\Lambda^2}{R_p}\right)\omega \tag{44}$$

and

$$T = 0 \tag{45}$$

respectively.

When the expressions obtained in (44) and (45) are plotted on the torque-speed plane, we get one curve which is a straight line with negative slope and passes through the origin, and the other lies on the x axis as shown in Figure 16.

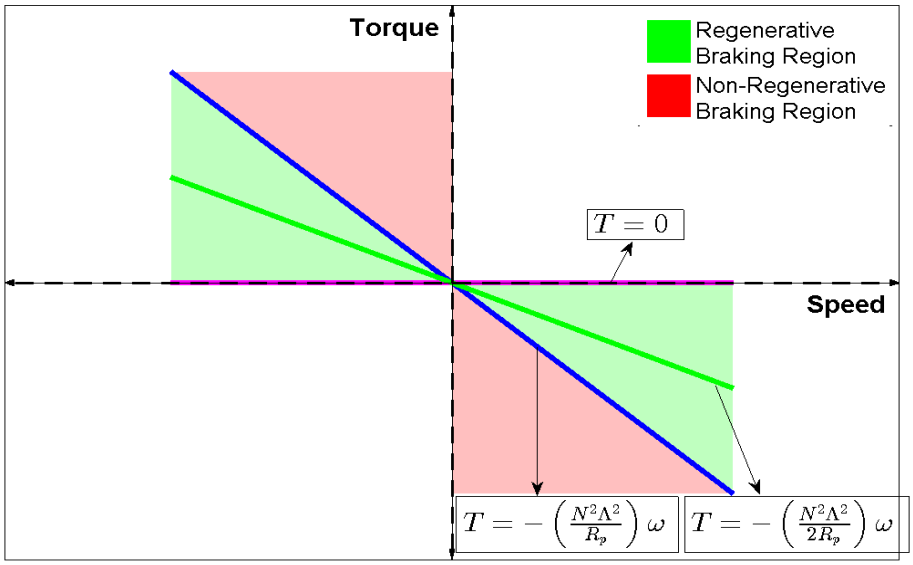

Figure 16: Regenerative braking boundaries and maximum regenerative braking current curve for a surface permanent magnet synchronous machine neglecting core loss resistance, R_c.

3.4.1.2 Maximum Regenerative Braking Current

In order to determine the maximum current absorbed by the DC source during regenerative braking, we minimize the electric power P_e with respect to the control currents i_d and i_q. The gradient vector is given as

$$\nabla P_e = \begin{bmatrix} \frac{\partial P_e}{\partial i_d} \\ \frac{\partial P_e}{\partial i_q} \end{bmatrix} = \begin{bmatrix} 2R_p i_d \\ N\Lambda\omega + 2R_p i_q \end{bmatrix}$$

Setting the gradient vector to zero, we obtain the values of i_d and i_q as

$$i_d = 0$$
$$i_q = -\left(\frac{N\Lambda}{2R_p}\right)\omega$$

The Hessian matrix of the optimization function P_e is computed as

$$\mathbf{H} = \begin{bmatrix} \dfrac{\partial P_e^2}{\partial i_d \partial i_d} & \dfrac{\partial P_e^2}{\partial i_d \partial i_q} \\ \dfrac{\partial P_e^2}{\partial i_q \partial i_d} & \dfrac{\partial P_e^2}{\partial i_q \partial i_q} \end{bmatrix} = \begin{bmatrix} 2R_p & 0 \\ 0 & 2R_p \end{bmatrix}$$

Since the Hessian matrix is positive definite symmetric, it can be concluded that the solution is a local minimum. The electromagnetic torque corresponding to the above current vector is

$$T = -\left(\frac{N^2\Lambda^2}{2R_p}\right)\omega \tag{46}$$

The expression in (46) is a straight line with a negative slope which is half of that of (44), and passes through the origin. Operation along this line will result in maximum current sent back to the DC source during regenerative braking and is given by

$$i_{s,\text{max regen}} = \frac{E_s - \sqrt{E_s^2 + N^2\Lambda^2\omega^2\left(\dfrac{R_s}{R_p}\right)}}{2R_s} \tag{47}$$

3.4.2 Including Core Loss Resistance, R_c

In this section, the core loss resistance is no longer neglected and the currents in the d and q circuits, i_d and i_q, split into two paths: the magnetizing components i_{dm} and i_{qm}, and the core loss components i_{cd} and i_{cq}. The expressions for the regenerative braking boundaries and maximum regenerative braking current for this case are developed as follows.

3.4.2.1 Regenerative Braking Boundaries

The electric machine loss is given as

$$W_{em} = (i_d^2 + i_q^2)R_p + (i_{cd}^2 + i_{cq}^2)R_c$$

where $i_{cd} = i_d - i_{dm}$ and $i_{cq} = i_q - i_{qm}$. The power balance equation is given as

$$\begin{aligned} P_e &= P_m + W_{em} \\ &= N\Lambda i_{qm}\omega + (i_d^2 + i_q^2)R_p + \left((i_d - i_{dm})^2 + (i_q - i_{qm})^2\right) R_c \end{aligned}$$

As seen earlier the regenerative boundary is obtained by setting $P_e = 0$. Applying this equality constraint and writing i_d and i_q in terms of i_{dm} and i_{qm} from (34), we get the current i_{qm} as a quadratic expression in terms of i_{dm}. The corresponding torque expression is a function of only one control variable, i.e. i_{dm}. In order to obtain the maximum and minimum regenerative braking torques, we find the gradient of the torque expression with respect to the control variable i_{dm} and set it to zero.

$$\begin{aligned} \frac{dT}{di_{dm}} &= 0 \\ \implies i_{dm} &= -\frac{N^2\omega^2\Lambda L\gamma\,(1+\gamma)}{R_p^2 + N^2\omega^2L^2\gamma\,(1+\gamma)} \end{aligned}$$

Using this value of i_{dm}, the expressions for i_{qm} are obtained as

$$i_{qm} = -N\Lambda\left(\frac{(1+\gamma)\,R_p}{R_p^2 + N^2\omega^2L^2\gamma\,(1+\gamma)}\right)\omega$$

and

$$i_{qm} = -N\Lambda\left(\frac{\gamma R_p}{R_p^2 + N^2\omega^2L^2\gamma\,(1+\gamma)}\right)\omega$$

where $\gamma = \dfrac{R_p}{R_c}$. The corresponding electromagnetic torques are

$$T = -N^2\Lambda^2\left(\frac{(1+\gamma)\,R_p}{R_p^2 + N^2\omega^2L^2\gamma\,(1+\gamma)}\right)\omega \tag{48}$$

and

$$T = -N^2\Lambda^2 \left(\frac{\gamma R_p}{R_p^2 + N^2\omega^2 L^2 \gamma \left(1+\gamma\right)} \right) \omega \tag{49}$$

respectively.

When plotted on the torque-speed plane, the above torque expressions represent two curves in the 4th and 2nd quadrants, (48) is close to the y axis and (49) is close to the x axis, as shown in Figure 17. The two curves divide each braking quadrant into three sections in the torque-speed plane. The two sections closer to the x and y axes correspond to regions where regenerative braking is not possible and the middle section corresponds to the region of regenerative braking.

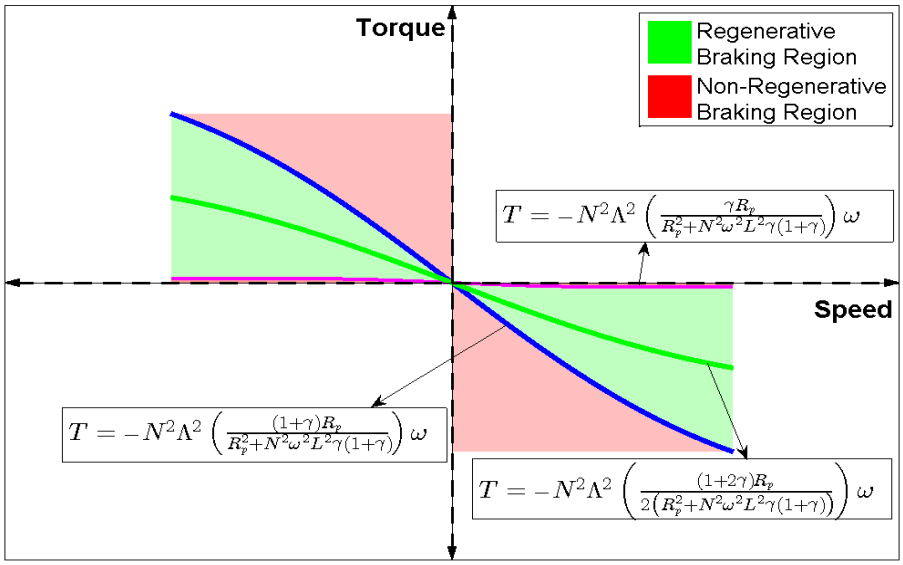

Figure 17: Regenerative braking boundaries and maximum regenerative braking current curve for a surface permanent magnet synchronous machine including core loss resistance, R_c.

3.4.2.2 Maximum Regenerative Braking Current

To determine the maximum current absorbed by the DC source during regenerative braking, P_e is minimized with respect to control currents i_{dm} and i_{qm}. The gradient

vector of the optimization function with respect to its control variables is computed using

$$\nabla P_e = \begin{bmatrix} \dfrac{\partial P_e}{\partial i_{dm}} \\ \dfrac{\partial P_e}{\partial i_{qm}} \end{bmatrix}$$

Setting the gradient vector to zero, we obtain the values of i_{dm} and i_{qm} as

$$i_{dm} = -\frac{N^2\omega^2\Lambda L\gamma\left(1+\gamma\right)}{R_p^2 + N^2\omega^2L^2\gamma\left(1+\gamma\right)}$$

$$i_{qm} = -N\Lambda\left(\frac{\left(1+2\gamma\right)R_p}{2\left(R_p^2 + N^2\omega^2L^2\gamma\left(1+\gamma\right)\right)}\right)\omega$$

The Hessian matrix is obtained as

$$\mathbf{H} = \begin{bmatrix} \dfrac{\partial P_e^2}{\partial i_{dm}\partial i_{dm}} & \dfrac{\partial P_e^2}{\partial i_{dm}\partial i_{qm}} \\ \dfrac{\partial P_e^2}{\partial i_{qm}\partial i_{dm}} & \dfrac{\partial P_e^2}{\partial i_{qm}\partial i_{qm}} \end{bmatrix}$$

$$= \begin{bmatrix} 2R_p + \dfrac{2N^2\omega^2L^2\gamma\left(1+\gamma\right)}{R_p} & 0 \\ 0 & 2R_p + \dfrac{2N^2\omega^2L^2\gamma\left(1+\gamma\right)}{R_p} \end{bmatrix}$$

The Hessian matrix is positive definite symmetric which is a necessary and sufficient condition to conclude that the solution is a local minimum. The torque corresponding to the above current vector is

$$T = -N^2\Lambda^2\left(\frac{\left(1+2\gamma\right)R_p}{2\left(R_p^2 + N^2\omega^2L^2\gamma\left(1+\gamma\right)\right)}\right)\omega \tag{50}$$

The expression for torque in (50) is a curve in the braking quadrants passing through the origin as shown in Figure 17. Operating along this curve will result in maximum current absorbed by the DC source during regenerative braking given by

$$i_{s,\text{max regen}} = \frac{E_s - \sqrt{E_s^2 + N^2\Lambda^2\omega^2\left(\dfrac{R_s}{R_p}\right)\beta}}{2R_s} \tag{51}$$

where

$$\beta = \frac{R_p^2}{R_p^2 + N^2\omega^2L^2\gamma(1+\gamma)}$$

The torque expressions in (48), (49) and (50) match the numerical solutions of the optimization problems, Problem 4, Problem 5 and Problem 6 respectively, for the surface mounted permanent magnet synchronous machine as shown in Figure 15. The curves match the numerical solutions in the low speed region where they lie within the torque-speed capability boundary. Beyond a certain speed, the curves representing the analytical solution exceed the torque-speed capability boundary and are forced to merge with it for the rest of the speed range.

Therefore, the expressions which describe the boundaries of regenerative braking and the maximum current absorbed by the DC source during regenerative braking have been derived for the surface mounted permanent magnet synchronous machine. This exercise provides a better understanding of the dependence of the boundaries of regenerative braking and maximum current absorbed during regenerative braking on system parameters. Just as seen earlier in the DC machine section, the expressions for the regenerative braking boundaries are independent of the DC source resistance. However, the DC source resistance does affect the overall torque-speed capability curves of the machine.

CHAPTER IV

APPLICATION IN AN ELECTRIC VEHICLE

The concept of regenerative braking is very important in the context of application in an electric or hybrid-electric vehicle since it represents recovering kinetic energy of the moving vehicle for storage in an energy storage system, like a battery, ultra-capacitor or flywheel. Every watt-hour of energy recovered by regenerative braking means that the electric vehicle can travel for a longer duration before the battery depletes its charge and a hybrid-electric vehicle consumes lesser fuel to travel a particular distance. An electric or hybrid-electric vehicle has the capability to brake both electrically using the electric machine and mechanically using friction brakes attached to the wheels. The friction brake system is generally designed to brake the vehicle to a safe stop even in the absence of electric braking. Though the braking event is a transient phenomenon for the vehicle, it is a steady-state operation for the electric machine which produces electric braking torque. This is because the time constant associated with the dynamics of the electric machine is very small compared to that associated with the dynamics of the vehicle which has a much larger inertia than the rotor of the electric machine.

Since electrical braking is used in combination with mechanical braking to provide the braking torque requested by the driver, this leads to the concept of braking strategy. As the electric machine braking assists the vehicle braking event, the mechanical friction brakes are subject to less wear and hence its components last longer. The braking strategy defines the rules to split the driver's braking command between the electric machine and mechanical friction brake system. This may impact the vehicle stability which is studied in [2], however this aspect is not considered in this thesis.

This chapter studies the impact of different vehicle braking strategies on the energy consumption measured at the energy storage system for an electric vehicle for a few commonly used test drive cycles. In order to determine the energy consumption of the vehicle, the total energy spent by the on-board energy storage system to traverse along the drive cycle must be determined. This requires modeling of the different power loss mechanisms that the vehicle and its components experience. The summation of these power losses along with the power required to accelerate and decelerate the vehicle along the drive cycle gives the total energy required from the energy storage system.

4.1 Loss Modeling

The total vehicle power losses are studied under electrical and mechanical subsystems. The electrical subsystem consists of one or more electric machines, the converter associated with each machine which connects it to the energy storage system, and the energy storage system itself. The mechanical system consists of the mechanical components of the vehicle such as tires, body, transmission, etc.

4.1.1 Electrical Subsystem Losses

Nowadays, the interior permanent magnet synchronous machine is widely used in electric and hybrid electric vehicle powertrains. Therefore, an electrical subsystem consisting of an interior permanent magnet synchronous machine, an inverter and DC source (an electrochemical battery pack) is studied. The losses associated with each individual component of the electrical subsystem are studied. It should be noted that the loss analysis of the above electrical subsystem is studied independent from its application in a vehicle.

From Figure 11, we can describe the electrical losses of an interior permanent

magnet synchronous machine under copper loss and iron (core) loss as

$$W_{Cu} = (i_d^2 + i_q^2)R_p$$

$$W_{Fe} = (i_{cd}^2 + i_{cq}^2)R_c$$

respectively. The total electric machine loss is written as

$$W_{em} = W_{Cu} + W_{Fe} \tag{52}$$

The concept of minimizing the combination of copper and iron losses, in a permanent magnet synchronous machine, while providing steady-state electromagnetic torque is established in [10]. This method of control is beneficial from an electric vehicle perspective since minimum machine loss results in lesser energy being extracted from the energy storage system. The copper and iron loss components of the electric machine loss shown in (52) can be minimized by controlling the machine currents. The mechanical friction loss associated with the bearings of the rotor has been neglected. The electric machine input power, P_{em}, is given as

$$P_{em} = T\omega + W_{em} = v_d i_d + v_q i_q \tag{53}$$

As discussed earlier, the inverter consists of three identical legs which are operated using pulse width modulation to produce a balanced three-phase output at the midpoints of the converter legs. The leg currents in the three legs are i_A, i_B and i_C. The duty ratio of the switches in the legs A, B and C are u_A, u_B and u_C as described earlier in Chapter 3. The PWM scheme chosen for the study adopts injection of third harmonics in order to maximally utilize the available DC-link voltage [11]. The inverter is assumed to be lossless for this study. This means that the conduction and switching losses of the semiconductor switches and diodes have been neglected.

$$W_{inv} = 0$$

The loss of the final electrical sub-component, the electrochemical battery pack, is modeled as

$$W_s = i_s^2 R_s$$

where R_s is the thevenin equivalent resistance of the battery pack and i_s is the battery current as shown in Figure 4.

The above expressions describing various losses associated with the electrical subsystem are summed up as W_e, which is the total loss associated with the electrical subsystem.

$$W_e = W_{em} + W_{inv} + W_s$$

We then define the following optimization problem:

Problem 7: minimize electrical loss W_e,

at specified operating point (T, ω),

subject to (34) and (35), $||u_{dq}|| \leq \max(U_{dq})$, $||i_{dq}|| \leq I_{\max}$

The above problem is solved for every operating point (T, ω) that lies within the torque-speed capability curve defined by the solutions of Problems 1 and 2 as shown in (36) and (37). The above problem was solved using numerical optimization function `fmincon` of the Optimization Toolbox in MATLAB for the system parameters described in Table 3.

The result of solving Problem 7 is shown in Figure 18, where the contours of loss in kilo-watts are plotted on the torque-speed plane. If the DC source power is $P_s = E_s i_s$ and the output mechanical power of the electric machine is $P_m = T\omega$, we can define the concept of system efficiency, η_s as

$$\eta_s = \begin{cases} \dfrac{P_m}{P_s}, & \text{if } P_m > 0 \text{ and } P_s > 0 \\ \dfrac{P_s}{P_m}, & \text{if } P_m < 0 \text{ and } P_s < 0 \\ 0, & \text{otherwise} \end{cases}$$

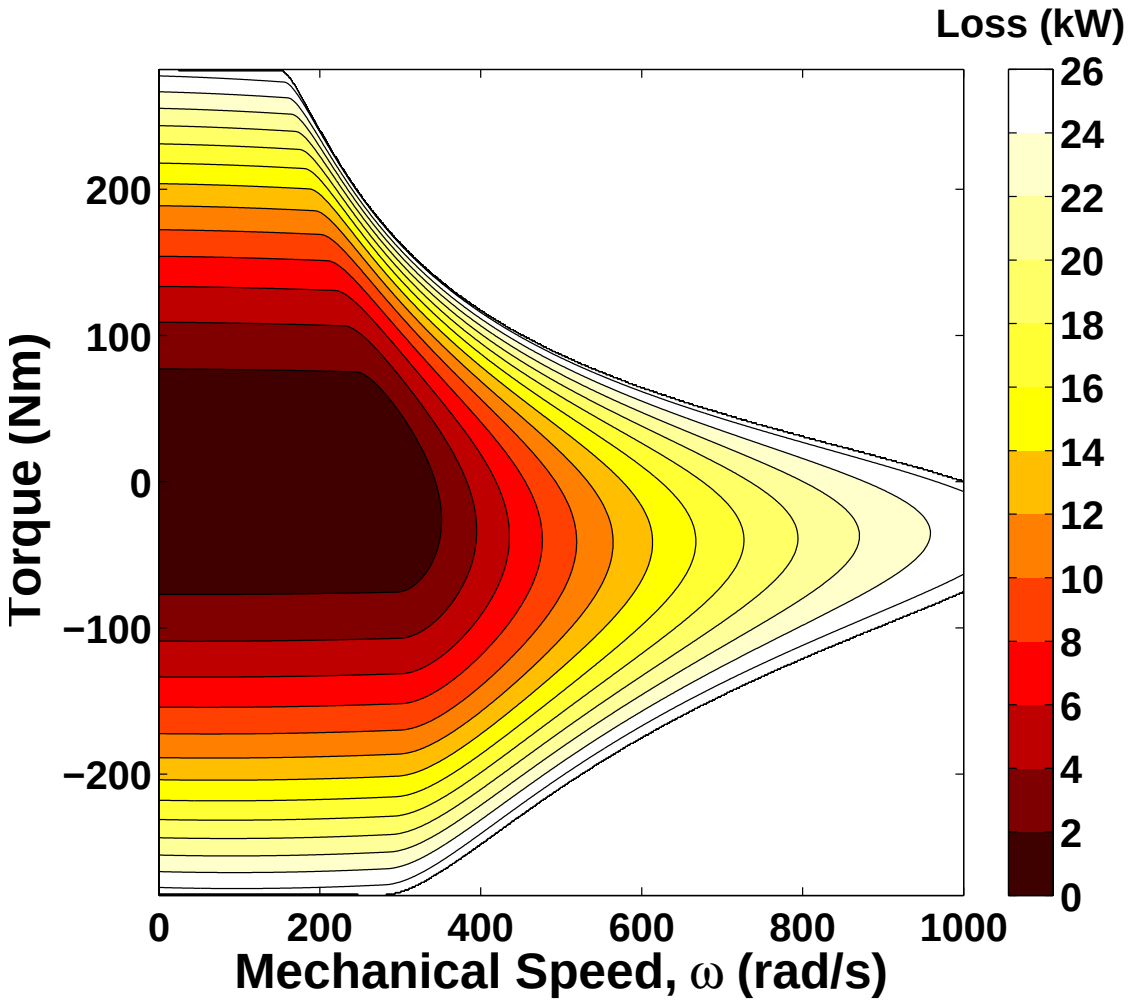

Figure 18: Contours of constant losses of the electrical subsystem plotted on the torque-speed plane.

The contours of efficiency on the torque-speed plane with the torque-speed capability curves, regenerative braking boundaries, and torque corresponding to maximum current absorbed by the DC source during regenerative braking, superimposed is shown in Figure 19. It can be seen that regions of non-regenerative braking described earlier correspond to zero efficiency. This is due to the fact that the DC source power $P_s > 0$ while electric machine mechanical power $P_m < 0$ for all operating points in the non-regenerative braking regions. This means that the DC source is spending energy to provide braking torque for operating points that fall in these regions.

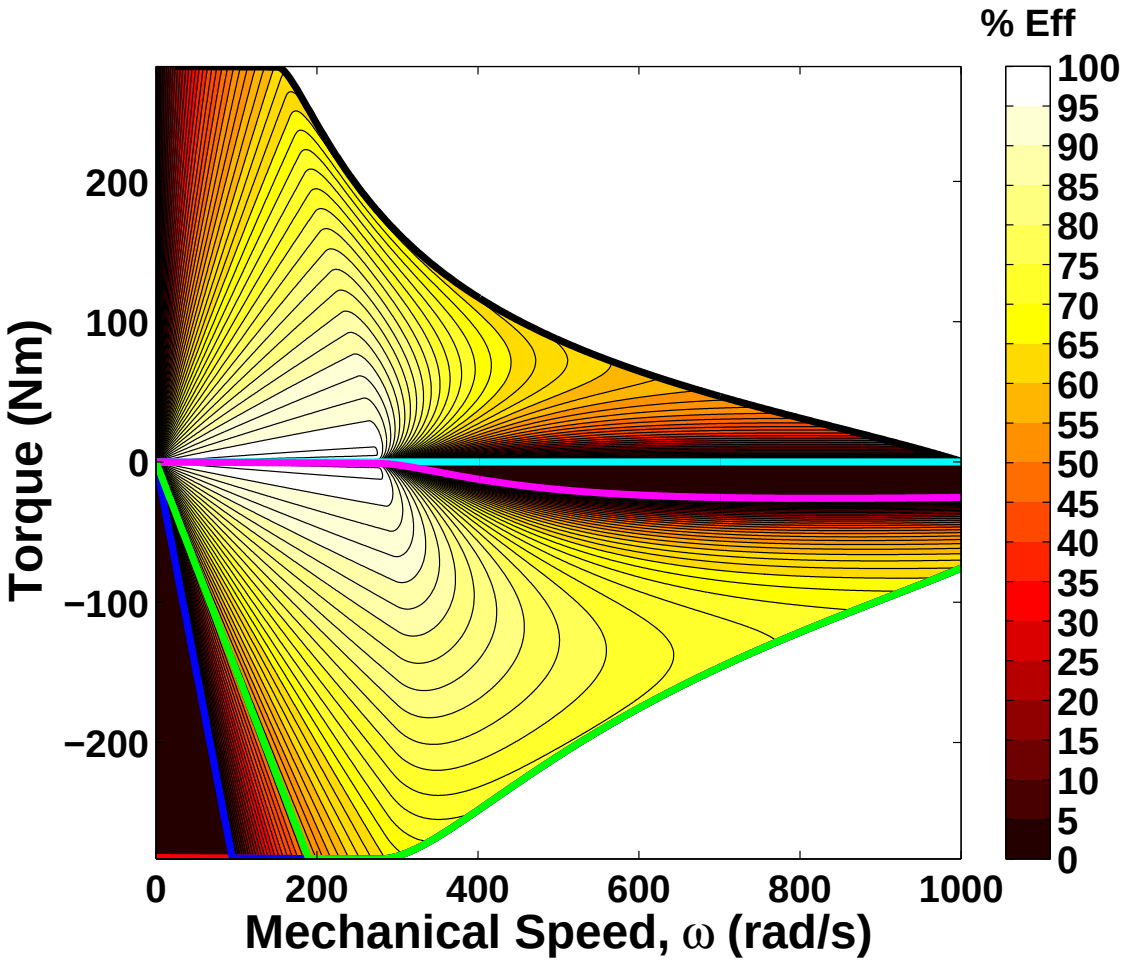

Figure 19: Contours of constant efficiency of the electrical subsystem plotted on the torque-speed plane.

4.1.2 Mechanical Subsystem Losses

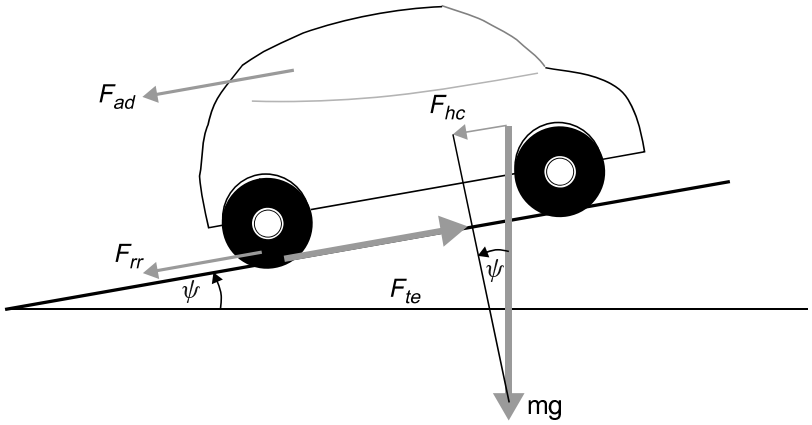

Figure 20: Resistance forces associated with a vehicle traveling along an inclined road.

A vehicle traveling on an inclined road is shown in Figure 20 [8]. The resistance forces associated with the vehicle are the road rolling resistance force,

$$F_{rr} = c_r mg,$$

the air drag resistance force,

$$F_{ad} = \frac{1}{2}\rho_a a_f c_d v_w^2,$$

and the hill climbing resistance force,

$$F_{hc} = mg\sin(\psi).$$

where c_r is the rolling resistance coefficient, m is the vehicle mass, g is the acceleration due to gravity, ρ_a is the density of air, a_f is the frontal area of the vehicle, c_d is the drag coefficient, v_w is the translation speed of the center of mass of the vehicle, which is referred to as vehicle speed from now on, and ψ is the inclination of the road surface. The vehicle's propulsion system has to provide power to overcome these forces in addition to accelerating or decelerating the vehicle. The acceleration or deceleration force is obtained by Newton's Second Law of Motion as

$$F_{acc} = (1 + \delta_m)m\frac{dv_w}{dt}$$

where δ_m is the dynamic mass factor of the vehicle. This factor accounts for the inertia of the various rotating components in the vehicle's powertrain and is generally a very small percentage of the vehicle's mass. The term $\frac{dv_w}{dt}$ is required acceleration or deceleration of the vehicle. The total tractive effort applied to the vehicle is written as

$$F_{te} = F_{rr} + F_{ad} + F_{hc} + F_{acc} \tag{54}$$

The on-board powerplant of the vehicle has to provide the above tractive effort to the wheels through a transmission system. If we consider an electric vehicle which has an electric machine as the only powerplant, then it has to provide the above tractive effort of the vehicle. The rotor of the electric machine is connected to the wheels through a gearing mechanism in the vehicle's transmission. The efficiency of the gearing mechanism is η_g, which gives a measure of the power loss in the gearing. If the wheel radius is r_w, then the torque required at the wheel is

$$T_w = F_{te} r_w$$

If the final drive gear ratio between the electric machine and wheel is i_g, then steady-state electromagnetic torque and mechanical speed of the rotor of the electric machine are given by

$$T = \frac{T_w}{i_g \eta_g}$$
$$\omega = \frac{i_g v_w}{r_w}$$

respectively.

Therefore, it can be seen that the vehicle's acceleration or deceleration request corresponds to a steady-state operating point on the electric machine's torque-speed plane.

4.2 Braking Strategies

An electric vehicle with an interior permanent magnet synchronous machine IPM-A, a lossless inverter and an electrochemical battery pack is considered. The machine's rotor is connected to wheel through a fixed gear. A drive cycle is a continuous set of desired vehicle speeds versus time that the vehicle has to follow. In order to achieve the desired acceleration or deceleration, the electric machine has to provide steady-state motoring or braking torque at a machine speed which is the vehicle speed scaled through a gear ratio in the vehicle's transmission. Therefore, each entry in the drive cycle data maps onto the electric machine torque-speed plane as a steady-state operating point, through a gear ratio. In this section we discuss braking strategies with respect to different sample operating points in the braking quadrant of the torque-speed plane of the electric machine.

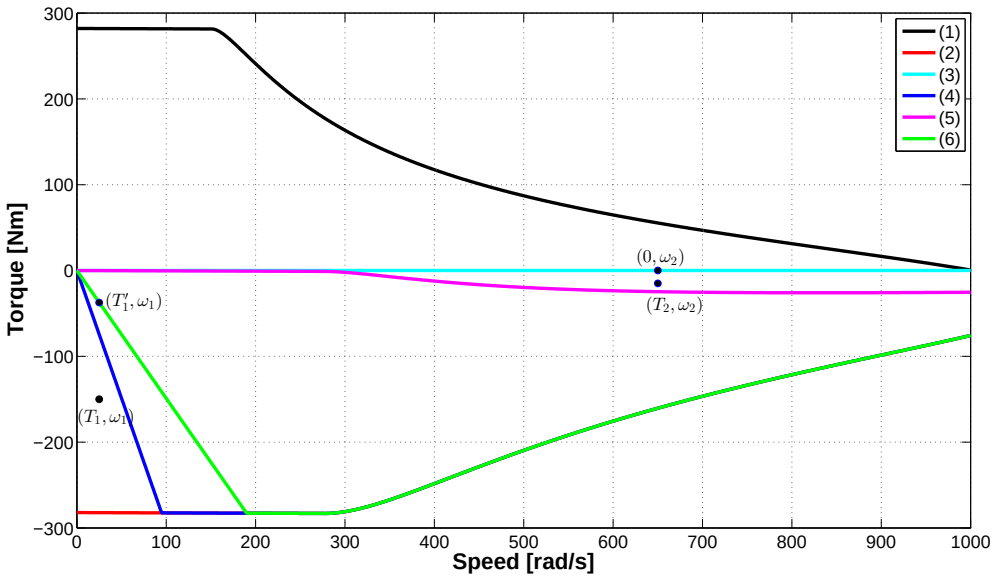

Figure 21: Sample operating points in the braking quadrant of the torque-speed plane used to explain the braking strategies.

Let (T_1, ω_1) represent an operating point as shown in Figure 21. This operating point lies in the electric machine's non-regenerative braking region which is adjacent

to the y axis. One option is to let the machine operate at this operating point but this would mean that the DC source is spending energy in order to brake the vehicle which depletes the energy it carries. Instead, the following braking strategy is proposed. Let (T_1', ω_1) be a point on the solution to Problem 6, as shown in Figure 21. This operating point is at the same machine speed as considered earlier, however this point is not only in the regenerative braking feasibility region, but also provides maximum current back to the DC source through regenerative braking. Therefore it is beneficial to shift the machine's operating point to (T_1', ω_1) and the remaining portion of vehicle braking torque is provided by mechanical friction brakes attached to the wheels. The value of the mechanical braking torque is given by

$$T_{mech} = (T_1 - T_1')\, i_g \eta_g$$

It should be noted that this strategy would apply to all operating points on the torque-speed plane of the electric machine that lie below the solution to Problem 6, whether or not they lie in the non-regenerative braking region.

It is also important to consider that the machine phase resistance is subject to change as the winding temperature varies. For example in the surface permanent magnet synchronous machine, it can be seen from (44) and (46), which represent the symbolic solutions to the regenerative braking feasibility boundary (Problem 4) and the maximum regenerative braking power absorbed by the DC source (Problem 6) respectively, that the curves are inversely proportional to machine phase resistance R_p. Also, it can be seen that the curve representing the solution to Problem 6 has a slope that is exactly half of that of the solution to Problem 4. In the absence of an instrument that accurately monitors the machine phase winding resistance, following the above braking strategy will always result in the machine operating within the regenerative braking feasibility region unless the winding temperature increases to such a degree so as to increase the phase resistance by more than 100%. But this temperature rise is practically impossible because it would exceed the temperature

ratings of typical wire insulating materials.

Another operating point of interest is (T_2, ω_2), which is a generic representation of all operating points that lie in the non-regenerative braking region close to the x axis as shown in Figure 21. Let P_{e2} be the electric power that is supplied to the machine to operate at this point. Since $P_{e2} > 0$, that is electric power is delivered to the machine to provide braking, it is not beneficial to operate at this point. We can consider shifting the operating point to the x axis at $(0, \omega_2)$ as shown in Figure 21, which has electric power $P'_{e2} > 0$ associated with it. This means the electric machine provides zero braking torque and all of the required vehicle braking torque is provided by the mechanical brakes for such operating points, which is another braking strategy. The mechanical braking torque is given by

$$T_{mech} = T_2 i_g \eta_g$$

Since this strategy involves moving the operating point further away from the $P_e = 0$ line, it would imply that

$$P'_{e2} > P_{e2} > 0$$

Therefore, the vehicle would consume more power operating at $(0, \omega_2)$ as compared to operating at (T_2, ω_2).

As discussed earlier, the objective is to study the impact on the vehicle's energy consumption using different braking strategies. The different braking strategies are summarized in Table 6.

4.3 Results

The above strategies were applied to a vehicle simulation for the following drive cycles obtained from the United States Environmental Protection Agency website [5],

- The EPA Urban Dynamometer Driving Schedule (UDDS)

Table 6: Braking Strategies

Braking Strategy	Description
Strategy I	Only mechanical brakes used. Electric machine used for motoring only.
Strategy II	Electric machine used for braking along with mechanical brakes. Operating points not shifted to optimize regenerative braking.
Strategy III	Electric machine used for braking along with mechanical brakes. (T_1, ω_1) shifted to (T_1', ω_1). (T_2, ω_2) shifted to $(0, \omega_2)$.
Strategy IV	Electric machine used for braking along with mechanical brakes. (T_1, ω_1) shifted to (T_1', ω_1). (T_2, ω_2) left unchanged.

- The Federal Test Procedure (FTP)
- The US06 which is a high acceleration aggressive driving schedule
- The New York City Cycle (NYCC)

Table 7: Vehicle Parameters

Mechanical Subsystem		Electrical Subsystem	
Parameter	Value	Parameter	Value
Vehicle mass (including driver and one passenger), m	1653.8 kg	Battery Pack Energy Capacity	24.72 kWh
Wheel radius, r_w	0.316 m	Battery Pack Voltage	366.3 V
Rolling resistance coefficient, c_r	0.0069	Battery Pack Charge Capacity	67.5 Ah
Drag coefficient, c_d	0.26	Battery Pack Resistance	0.0247 Ω
Frontal area of the vehicle, a_f	2.7435 m^2	Initial State of Charge	90%
Dynamic Mass Factor, δ_m	4%	Electric Machine	Table 3
Gear Ratio, i_g	8.125		
Gear Efficiency, η_g	95%		

The vehicle parameters used for the simulations are shown in Table 7. Simulations were run for one cycle of each driving schedule using each of the braking strategies

discussed in Table 6 and the energy consumption at the end of each drive cycle was tabulated as shown below in Table 8.

Table 8: Simulation Results

Drive Schedule	Energy Consumption (Wh/mile)			
	Strategy I	Strategy II	Strategy III	Strategy IV
UDDS	320.83	227.29	231.86	226.92
FTP	352.93	260.73	266.71	260.39
US06	689.89	593.67	602.57	593.32
NYCC	328.40	158.39	157.50	157.44

Figure 22 shows the vehicle's operating points superimposed on the efficiency contour map of the electrical subsystem. The shift of operating points in the braking quadrant while adopting different braking strategies can clearly be noticed. From Table 8, it can be seen that it is beneficial to use electric braking from the electric machine to assist the mechanical braking system to provide the requested vehicle braking torque (Strategy II), since it reduces the energy consumption by a huge amount. Furthermore, Strategy IV results in a reduction in energy consumption of about $0.3 - 1.1$ Wh/mile compared to Strategy II. A 100 mile excursion saves $0.03 - 0.11$ kWh of the energy storage system's net energy. Strategy III does not provide any benefit and in fact causes an increase in energy consumption. This can be explained by referring back to Figure 21. As explained earlier, P_{e2} is the electric power that is supplied to the machine to operate at a non-regenerative braking point (T_2, ω_2) (i.e. Strategy II) and P'_{e2} is the electric power that is supplied to the machine to operate at $(0, \omega_2)$ (i.e. Strategy III), it follows that $P'_{e2} > P_{e2} > 0$. This means that the DC source supplies more power to operate at $(0, \omega_2)$ than at (T_2, ω_2), which is a more detrimental situation.

We can conclude that for this simplistic vehicle architecture which involves only one electric machine driving the wheel through a fixed gear ratio, it is most beneficial

to adopt Strategy IV. Though we do not see a lot of energy being saved compared to Strategy II, the simplistic nature of the vehicle architecture does not permit implementation of more complex braking strategies. In other vehicle architectures such as series, parallel or power-split hybrid electric vehicles, which involve multiple powerplants such as internal combustion engines and one or more electric machines, more complex braking strategies can be envisioned to reduce energy consumption. Therefore, recognition of the regenerative braking feasibility boundaries (Problems 4 and 5) and the curve describing the maximum current absorbed by the DC source (Problem 6) and incorporation of braking strategies leads to a reduction in the energy consumption of an electric or hybrid-electric vehicle.

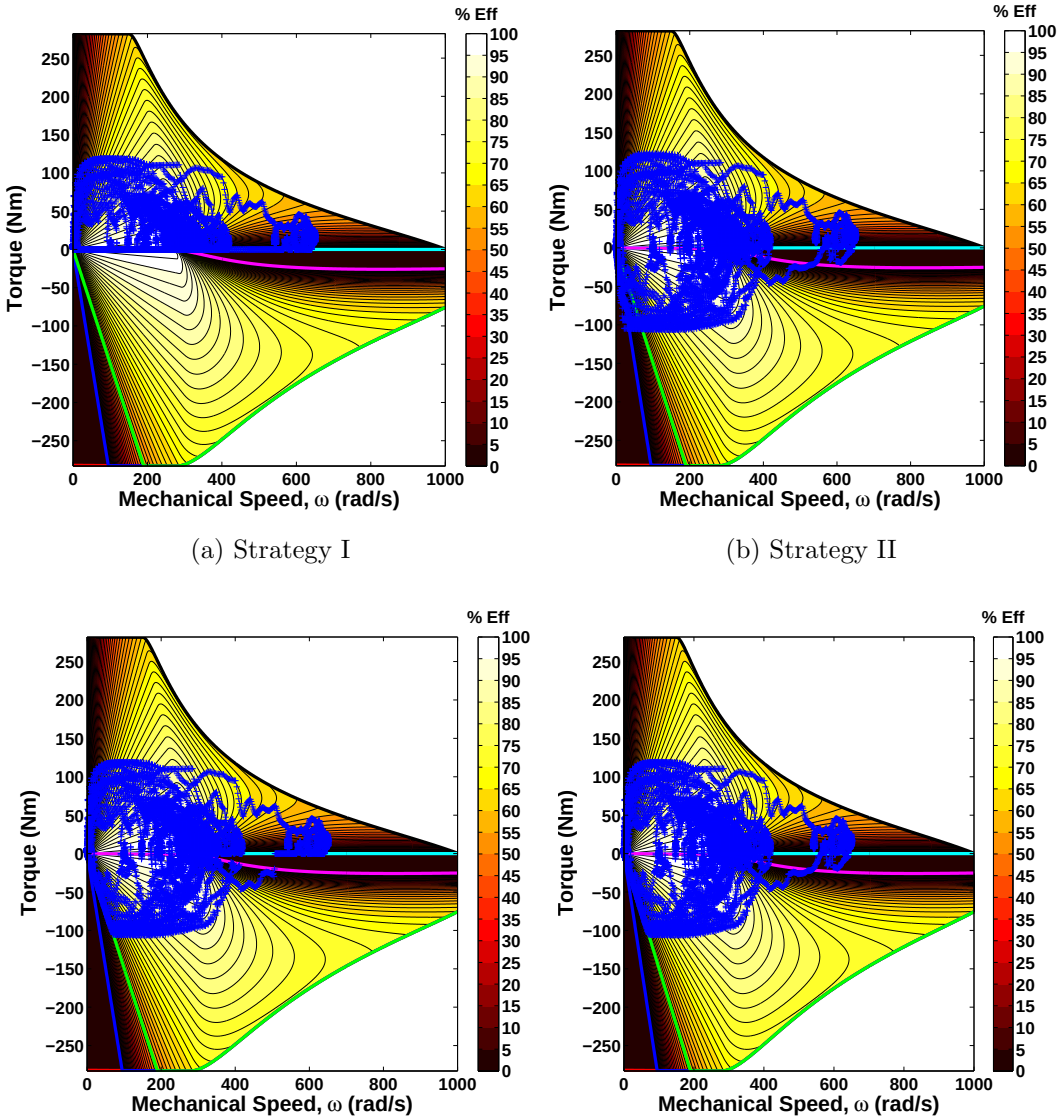

(a) Strategy I

(b) Strategy II

(c) Strategy III

(d) Strategy IV

Figure 22: Comparison of braking strategies for the UDDS drive cycle

CHAPTER V

CONCLUSION

The braking quadrants in the torque-speed plane of an electric machine are divided into regenerative and non-regenerative braking regions. This was seen in the numerical method of analysis for the separately excited DC machine, permanent magnet DC machine and permanent magnet synchronous machines. There also exists a curve which describes the maximum current absorbed by the DC source during regenerative braking. Symbolic expressions which describe the boundaries of regenerative braking and maximum regenerative braking current curve were obtained for the permanent magnet DC machine. It was found that the expressions obtained were dependent only on the machine's armature and core-loss resistances and magnetic constant, and were independent of the DC source parameters.

For permanent magnet synchronous machines, it was found that the shape of the curves describing the boundaries of regenerative braking and maximum regenerative braking current were different for the two interior permanent magnet synchronous machines that were studied. Symbolic expressions which describe the above curves for a surface permanent magnet synchronous machine were obtained. It was found that the expressions for the curves depend only on the machine parameters and not on the DC source parameters in this case as well.

When electric machines are used in vehicular applications, it is important to consider the boundaries of regenerative braking. If the vehicle driving condition places the machine's steady-state operating point in the non-regenerative braking regions, braking strategies are devised to minimize vehicle energy consumption. For the simple vehicle architecture which uses only one electric machine connected to the wheels

through a fixed gear ratio, different braking strategies were compared for energy consumption along various driving schedules. Braking strategy IV described in Table 6 was found to consume the least amount of energy from the DC source for this vehicle architecture. Vehicle architectures that involve multiple powerplants like internal combustion engines and electric machines such as series, parallel and power-split hybrid electric vehicles would require more complex braking strategies depending on the location of steady-state operating points in the braking quadrants of the machines' torque-speed planes. Therefore, recognition of the regenerative braking feasibility boundaries and the curve describing the maximum current absorbed by the DC source is an important step in devising braking strategies to minimize the energy consumption of electric and hybrid-electric vehicles.

REFERENCES

[1] Chen, C.-H., Chi, W.-C., and Cheng, M.-Y., "Regenerative braking control for light electric vehicles," in *2011 IEEE Ninth International Conference on Power Electronics and Drive Systems (PEDS)*, pp. 631 – 636, Dec 2011.

[2] Cikanek, S. and Bailey, K., "Regenerative braking system for a hybrid electric vehicle," in *Proceedings of the 2002 American Control Conference*, vol. 4, pp. 3129 – 3134, 2002.

[3] Crombez, D. and Czubay, J., "Vehicle and method for controlling regenerative braking." Patent, US 0303498 A1, Dec 2011.

[4] Dubey, G. K., *Fundamentals of Electrical Drives*. Alpha Science International Ltd., 2002.

[5] Environmental Protection Agency, U. S., "Dynamometer drive schedules." http://www.epa.gov/nvfel/testing/dynamometer.htm, 2013.

[6] Hua, L., Meng-chun, Z., Jian, Z., Da, X., and Hai, L., "Study on regenerative brake method of hybrid electric drive system of armored vehicle," in *2011 First International Conference on Instrumentation, Measurement, Computer, Communication and Control*, pp. 970 – 973, Oct 2011.

[7] Kangkang, Z., Jianqiu, L., Minggao, O., Jing, G., and Yan, M., "Electric braking performance analysis of pmsm for electric vehicle applications," in *2011 International Conference on Electronic and Mechanical Engineering and Information Technology (EMEIT)*, vol. 5, pp. 2596 – 2599, Aug 2011.

[8] Larminie, J. and Lowry, J., *Electric Vehicle Technology Explained*. John Wiley & Sons, 2004.

[9] Luo, G., Chen, Z., Deng, Y., Dou, M., and Liu, W., "Research on braking of battery-supplied interior permanent magnet motor driving system," in *Vehicle Power and Propulsion Conference, 2009. VPPC '09. IEEE*, pp. 270 – 274, Sept 2009.

[10] Morimoto, S., Tong, Y., Takeda, Y., and Hirasa, T., "Loss minimization control of permanent magnet synchronous motor drives," *IEEE Transactions on Industrial Electronics*, vol. 41, pp. 511 – 517, Oct 1994.

[11] Schoenen, T., Krings, A., van Treek, D., and De Doncker, R., "Maximum dc-link voltage utilization for optimal operation of ipmsm," in *Electric Machines and Drives Conference, 2009. IEMDC '09. IEEE International*, pp. 1547 – 1550, May 2009.

[12] Wang, F., Yin, X., Luo, H., and Huang, Y., "A series regenerative braking control strategy based on hybrid-power," in *2012 International Conference on Computer Distributed Control and Intelligent Environmental Monitoring (CDCIEM)*, pp. 65 – 69, Mar 2012.